ENGINEERING STATIC AND DYNAMIC CONTROL OF MICROBIAL BIOSYNTHETIC PATHWAYS IN *ESCHERICHIA COLI*

by

YAPING YANG

(Under the Direction of Yajun Yan)

ABSTRACT

In metabolic engineering, control of native metabolism is significant when optimizing strains for overproduction of the desired compounds in the selected host strains. However, for many central metabolic pathway genes, static knockout strategies result in poor cell growth and gene expression. To address this problem, we have engineered antisense RNAs to achieve conditionally static repression of multiple genes in fatty acid biosynthesis pathway to increase the malonyl-CoA pool and improve the bioproduction of malonyl-CoA-derived compounds. Inspired from naturally-existed dynamic regulatory systems, we engineered an artificial dynamic control network to dynamically regulate the exogenous pathways and the endogenous metabolic network in an orthogonal manner, permitting maximum utilization of carbon source. Furthermore, we anchored this dynamic control system into the muconic acid (MA) biosynthesis pathway to test its applicability. This research provided a proof-of concept demonstrating static and dynamic control of the gene expression, enriched new yield optimization approvals and supplied a theoretical basis for biosynthesis research.

INDEX WORDS: Metabolic engineering; Static control; asRNA; Dynamic control network

# ENGINEERING STATIC AND DYNAMIC CONTROL OF MICROBIAL BIOSYNTHETIC PATHWAYS IN *ESCHERICHIA COLI*

by

YAPING YANG

B.E., Tianjin University of Science and Technology, China, 2008

M.S., Nankai University, China, 2012

A Dissertation Submitted to the Graduate Faculty of The University of Georgia in Partial Fulfillment of the Requirements for the Degree

DOCTOR OF PHILOSOPHY

ATHENS, GEORGIA

2017

# ENGINEERING STATIC AND DYNAMIC CONTROL OF MICROBIAL BIOSYNTHETIC PATHWAYS IN *ESCHERICHIA COLI*

by

YAPING YANG

Major Professor: Yajun Yan

Committee: William B Whitman
Williams Kisaalita
James Kastner

Electronic Version Approved:

Suzanne Barbour
Dean of the Graduate School
The University of Georgia
December 2017

# DEDICATION

I would like to dedicate to this dissertation to my husband Hongfei Yan and my daughter Caitlin Y Yan.

ACKNOWLEDGEMENTS

I would like to express my sincere gratitude to my major professor Dr. Yajun Yan, who guides me to form the rigorous research attitude and conducts me the most comprehensive technical training and the in-depth brainstorming. With his profound knowledge and extreme patience, he led me out of every research bottleneck and encouraged me to continue my research work during my Ph.D. period. Without his guidance, this dissertation would not have been possible.

I sincerely thank my committee members, Dr. William B Whitman, Dr. Williams Kisaalita and Dr. Jim Kastner for their guidance and encouragement in carrying out this project.

I also wish to express my gratitude to all the lab members who rendered their help during my research.

Finally, I want to thank my family for their selfless support.

TABLE OF CONTENTS

Page

LIST OF TABLES

Page

LIST OF FIGURES

Page

# CHAPTER 1

## INTRODUCTION

Cellular metabolism in microbes is a tightly regulated metabolic network. By monitoring the needs and surpluses among different metabolic pathways, microorganisms can globally control carbon flow to maintain the cell growth in an economical and effective mode[1]. Further understanding of the metabolic regulation mechanisms has enabled researchers to manipulate and redesign the intrinsic metabolic network toward a defined objective, such as overproducing the desired compounds[2]. A number of permanent genetic modification strategies have been commonly used to improve the microbial producers, such as overexpressing rate-limiting enzymes, deleting competing pathways and eliminating undesired endogenous regulations[3-5]. While these strategies have achieved desired success, the production efficiency of microbial producers is frequently compromised due to unexpected metabolic imbalance. For example, maximizing the product pathway flux can drain the metabolites from the biomass synthesis to the production of desired compounds, leading to slow growth rates. To balance metabolic pathways, some other static fine-tuning strategies are developed by adjusting gene copy numbers, tuning promoter strengths, changing RBS sites, optimizing operon organizations and localizing enzymes by protein scaffolds or compartmentalization, etc[5-8]. Even though these strategies are proven effective, the static control is usually manipulated for a specific condition. Any cellular and environmental changes may influence microbial production due to the lack of dynamic response to cellular and environmental changes[9].

Compared with the static control, native metabolic pathways use dynamic regulatory networks to respond to the changing psychological or environmental conditions by altering fluxes in real-time[10]. Inspired by the mechanism of natural metabolism, researchers have begun to adopt dynamic regulatory machinery to design the engineered microbes for the production of value-added chemicals. So far, only a few successful cases has been reported. For instance, Farmer and Liao firstly reported the development of a promoter-regulator system which can sense acetyl phosphate, an indirect indicator of the excess glycolytic flux in *E. coli*[11]. This system could dynamically upregulate the expression of two genes (*pps* and *idi*), allowing the carbon flux to be rerouted to lycopene biosynthesis. Recently, Keasling et al. engineered a promoter-regulator system which could sense the key intermediate (oleic acid) and was used to dynamically control ethanol biosynthesis, fatty acid biosynthesis, and esterification modules, resulting in the increase of biodiesel production in *E. coli*[12]. Similarly, Koffas et al. developed a promoter-regulator system which could sense malonyl-CoA, a key metabolite in the fatty acid biosynthesis pathway, to dynamically control the production of the fatty acid-derived compounds[13]. Conclusively, these demonstrated applications applied a sensor regulator to control the pathway genes. When the metabolites accumulated, they were sensed as signal to up-regulate the desired pathway genes.

These strategies have exhibited effectiveness in alleviating metabolic imbalances, however, some limitations still exist. First, the promoter-mediated regulation systems are mono-functional, which usually allows effective up-regulation but less efficient down-regulation. Second, the reported dynamic regulations were limited to the pathway enzymes under the control of responsive promoters. They cannot control the host cells' native genes located on the chromosome where down-regulation is needed. Additionally, the physiological changes of host cells at the early stage of cell growth were not taken into consideration in previous dynamic

regulation designs. In fermentation processes, cells usually experience a lag phase after inoculation into the fermentation media. This transitional period prepares the cells for exponential growth. The overexpression of heterologous enzymes at an early stage of cell growth and/or deletion of native genes frequently leads to significant growth retardation and inhibition because engineered pathways compete with native metabolism for the limited cell resources[14]. Poor cell adaption into the fermentation media may exert significant negative effects in the entire microbial production process[15]. Thus, an ideal manipulation strategy is to maintain native metabolism intact and keep exogenous pathway enzymes being turned off during the cell lag phase, allowing host cells to adapt to the fermentation environment undisturbedly. As cells get adapted and enter the exponential phase, we expect the expression of heterologous enzymes to be turned up gradually to a high level and the native competing pathways to be turned down so that maximal carbon flow is directed to the target product.

The following chapters present two cases of engineering static and dynamic control of microbial biosynthesis pathways to enhance bioproduction in *E. coli*. In chapter 2, we engineered antisense RNA strategy to achieve static repression of multiple genes in fatty acid biosynthesis pathway to increase malonyl-CoA pool and improve malonyl-CoA based bioproduction. Based on the robust performance of asRNA strategy in repressing gene expression, in chapter 3, we report a standard protocol of asRNA design and provide valuable notes in the further experimental operation to guide peer researchers. In chapter 4, we describe an artificial dynamic control network to dynamically regulate the exogenous pathways and the endogenous metabolic network in an orthogonal manner, permitting maximum utilization of carbon source. Furthermore, we use the muconic acid (MA) biosynthesis pathway as a proof-of-concept demonstration to test the applicability of such an artificial regulatory network and significantly

enhance the muconic acid production to 1.8 g/L, which is substantially higher than the static controls. These chapters are relatively independent with each other. Each work includes the design, validation and optimization of a control system to improve its applicability in the artificial biosynthesis pathway and improve the relative bioproduction. This research provides static and dynamic control of the gene expression, enriched new yield optimization approvals and supplied a theoretical basis for biosynthesis research.

# CHAPTER 2[1]

REGULATING MALONYL-COA METABOLISM VIA SYNTHETIC ANTISENSE RNAs

FOR ENHANCED BIOSYNTHESIS OF NATURE PRODUCTS

[1] Yaping Yang[1], Yuheng Lin[1], Lingyun Li, Robert J. Linhardt, Yajun Yan. 2015. Metabolic Engineering. 29: 217-226.
Reprinted here with permission of the publisher.

## 2.1 Abstract

Malonyl-CoA is the building block for fatty acid biosynthesis and also a precursor to various pharmaceutically and industrially valuable molecules, such as polyketides and biopolymers. However, intracellular malonyl-CoA is usually maintained at low levels, which poses great challenges to efficient microbial production of malonyl-CoA derived molecules. Inactivation of the malonyl-CoA consumption pathway to increase its intracellular availability is not applicable, since it is usually lethal to microorganisms. In this work, we employ synthetic antisense RNAs (asRNAs) to conditionally down-regulate fatty acid biosynthesis and achieve malonyl-CoA enrichment in *Escherichia coli*. The optimized asRNA constructs with a loop-stem structure exhibit high interference efficiency up to 80%, leading to a 4.5-fold increase in intracellular malonyl-CoA concentration when *fabD* gene expression is inhibited. Strikingly, this strategy allows the improved production of natural products 4-hydroxycoumarin, resveratrol, and naringenin by 2.53-, 1.70-, and 1.53-fold in *E. coli*, respectively. In addition, down-regulation of other *fab* genes including *fabH*, *fabB*, and *fabF* also leads to remarkable increases in 4-hydroxycoumarin production. This study demonstrates a novel strategy to enhance intracellular malonyl-CoA and indicates the effectiveness of asRNA as a powerful tool for use in metabolic engineering.

## 2.2 Introduction

Malonyl-CoA is a universal building block not only for fatty acid biosynthesis, but also for the formation of a variety of natural products, such as coumarins, stilbenes, flavonoids and tetracyclines [1], which have been broadly used as pharmaceuticals and nutraceuticals with various health promoting effects. These compounds are usually generated as secondary metabolites in

plants or microorganisms by polyketide synthases (PKSs) through the repeated condensation of various numbers of malonyl-CoA(s) to different starter molecules [17-21]. For example, 4-hydroxycoumarin, a direct precursor to the widely used anticoagulant warfarin, can be biosynthesized through the condensation of one molecule of malonyl-CoA with salicoyl-CoA; while the formation of naringenin (the gateway molecule to flavonoids) and resveratrol (a representative of stilbene polyphenols) involves the condensation of three malonyl-CoA molecules with *p*-coumaroyl-CoA [17-19, 22]. Additionally, tetracyclines and doxorubicin, type II polyketides functioning as potent antibiotics and anti-cancer drugs, require eight and nine malonyl-CoA units for their biosynthesis, respectively [17, 19].

Due to the intrinsic disadvantages associated with their natural producers, such as low productivity, low growth rate, high cultivation cost, and lack of facile genetic tools, growing attention has been placed on developing heterologous microbial cell factories towards economically viable production of these compounds. So far, *Escherichia coli* is still the most preferred host microorganism because of its favorable fermentation properties and ease of genetic manipulation [23]. In fact, many malonyl-CoA derived natural products have been successfully produced by metabolically engineered *E. coli*, such as 4-hydroxycoumarin, resveratrol, naringenin, phloroglucinol, 7-*O*-methyl aromadendrin, genistein, and daidzein [17-19, 24-26]. In addition, a malonyl-CoA dependent pathway has been constructed for the production of 3-hydroxyproionic acid, an industrially valuable molecule ranked among top of the platform chemicals derived from biomass [27].

However, intracellular malonyl-CoA concentration is usually tightly regulated and maintained at very low levels, which poses great limitation in the productivity of malonyl-CoA derived molecules [28]. Therefore, enrichment of intracellular malonyl-CoA pool is of paramount

importance for their efficient production. In *E. coli*, malonyl-CoA level is directly determined by the balance of the upstream biosynthesis pathway and the downstream consumption pathway towards fatty acid biosynthesis (Figure 2.1a). Previous efforts to improve malonyl-CoA availability were mainly focused on engineering the upstream pathway, such as over-expression of acetyl-CoA carboxylase (ACC) to increase the conversion of acetyl-CoA into malonyl-CoA [13, 29], over-expression of acetyl-CoA synthase to enhance acetyl-CoA supply, and deleting acetyl-CoA consumption pathways involved in ethanol and acetate production [30]. In contrast, few efforts have been made in engineering the malonyl-CoA consumption pathway, since inactivation of fatty acid biosynthesis through conventional gene knockout strategies is usually lethal to host cells [31]. Only limited attempts have been reported to use certain antibiotics to inhibit fatty acid biosynthesis. For example, cerulenin, a specific inhibitor to the β-ketoacyl-acyl carrier protein synthases (KAS) I and II (FabB and FabF) [32], has been employed to improve the production of polyketides [21, 23, 33]. However, the use of such antibiotics is usually very costly and, thus, infeasible for application in large-scale production. Here we develop a powerful and inexpensive strategy using antisense RNAs instead of antibiotics to conditionally inhibit fatty acid biosynthesis and reduce undesired malonyl-CoA consumption to overcome this limitation.

Antisense RNAs (asRNAs) are single-stranded RNAs that can complementarily pair with their target mRNA and inhibit gene expression [34]. In plants and yeast, they have been exploited and they exhibit bright prospects as an essential tool to make up the shortcomings of conventional gene knockout strategies [35, 36]. However, in bacteria, even though small regulatory RNAs (srRNAs) have been reported, the application of naturally existing asRNAs on the regulation of gene expression has been limited [37, 38]. Most reports focus on the design of artificial, synthetic asRNAs and their use in identifying functional genes [39], verifying antibacterial mechanisms [40],

changing antibiotic susceptibility [41], examining rate-limiting genes [42], and regulating gene expression as a riboswitch [43]. Despite these exciting achievements, only a few studies have been reported on the metabolic engineering application of asRNAs. Lee's group successfully screened and utilized asRNAs to target 130 library genes, and dramatically improved tyrosine and cadaverine production. Based on the effectiveness of the Hfq scaffold protein, this asRNA structure was expected to be exploited as a tool to modulate gene expression in *E. coli* [44, 45]. Prather's group reported the engineering of asRNAs as a metabolite valve to dynamically control central carbon [46]. Another study investigated the use of asRNA (RyhB) to improve succinate production in *E. coli* [47].

In this work, we further explore and expand the application of asRNAs to target the genes and pathways that are essential for cell viability. We employ an artificial loop-stem scaffold carrying asRNAs and develop them as a tool for down-regulating genes involved in fatty acid biosynthesis. Optimization of asRNA binding lengths results in high interference efficiency (up to 80% inhibition of target gene expression). The engineered *E. coli* strain with *fabD* interfered by its asRNA *asfabD*(100) shows a 4.5-fold increase in intracellular malonyl-CoA concentration. On this basis, the biosynthetic pathways of 4-hydroxycoumarin, resveratrol, and naringenin are introduced into the *fabD*-interfered strain, which leads to significant improvement in their production. In addition, other critical genes involved in fatty acid biosynthesis *fabH*, *fabF*, *fabB* are also targeted with their respective asRNAs, leading to the enhanced production of malonyl-CoA derived 4-hydroxycoumarin as well. This work demonstrates an effective strategy to enhance malonyl-CoA availability and suggests the great potential of asRNAs for metabolic engineering use, especially for down-regulating the expression of those genes that are essential for cell viability.

## 2.3 Materials and Methods

### 2.3.1 Experimental materials

Luria-Bertani (LB) medium was used to grow *E. coli* cells for plasmid construction, propagation and inoculum preparation. The biosynthesis medium M9Y contains (per liter): glycerol (20 g), yeast extract (5 g), $NH_4Cl$ (1 g), $Na_2HPO_4$ (6 g), $KH_2PO_4$ (3 g), NaCl (0.5 g), $MgSO_4 \cdot 7H_2O$ (2 mmol), $CaCl_2 \cdot 2H_2O$ (0.1mmol) and vitamin B1 (1.0 mg). Ampicillin (100 mg/L), kanamycin (50 mg/L), and/or chloramphenicol (34 mg/L) were added to cultures when necessary. *E. coli* strain XL1-Blue was used for plasmid propagation and gene cloning; BW25113 was used as the host strain for the biosynthesis of 4-hydroxycoumarin, resveratrol and naringenin. Plasmids pZE12-luc, pCS27 and pSA74 are high, medium, and low-copy number plasmids employed for gene cloning, protein expression and pathway assembly in this work [48-50]. Table 2.1 lists the strains and plasmids used in this study.

eGFP cDNA (GenBank accession number U55762) was a kind gift from Dr. Gang Cheng group at the Chemical and Biomolecular Engineering Department of University of Akron (OH). The cDNAs of 4CL2 from *Petroselinum crispum*, STS from *Vitis vinifera*, CHI from *Medicago sativa* and CHS from *Petunia hybrida* were generous gifts from Dr. Koffas group at Rensselaer Polytechnic Institute (NY) [51-55].

Phusion High-Fidelity DNA polymerase, DNase I, restriction endonucleases, Quick Ligation Kit and Protoscript II first strand cDNA synthesis kit were purchased from New England Biolabs (Beverly, MA, USA). Zyppy™ Plasmid Miniprep Kit, Zymoclean™ Gel DNA Recovery Kit,

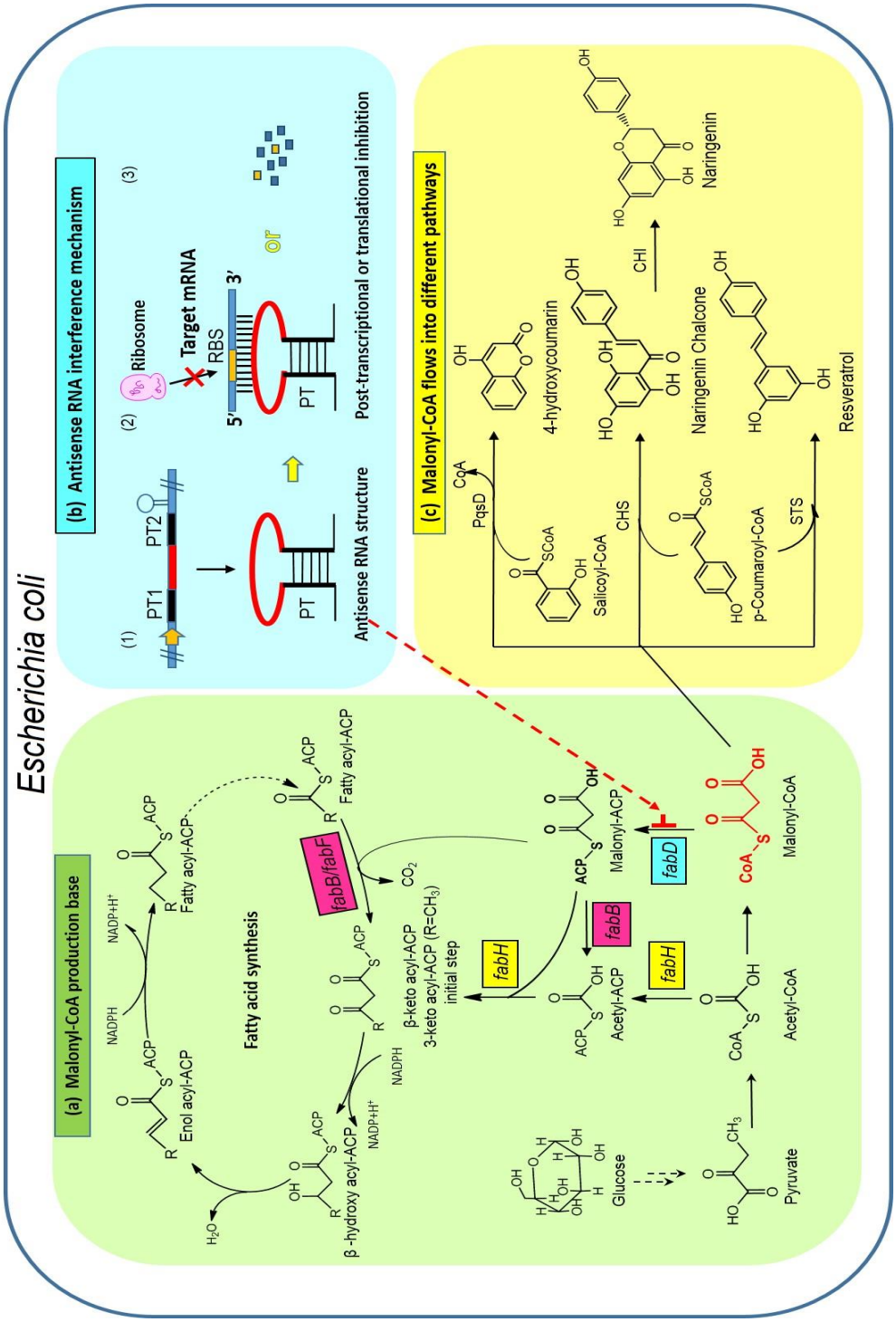


**Figure 2.1** Engineering of *E. coli* malonyl-CoA metabolic pathways. (a) Malonyl-CoA metabolic networks. *fabD*, encoding malonyl-CoA: ACP transacylase; *fabH*, encoding β-

ketoacyl-ACP synthase III; *fabB*, encoding β-ketoacyl-ACP synthase I; *fabF*, encoding β-ketoacyl-ACP synthase II. (b) asRNA interference mechanism. (1) Generation of mature asRNA from DNA (2) Binding of asRNA to its target mRNA. (3) Degradation of target mRNA. (c) malonyl-CoA fluxes into different polyketide pathways.

and DNA Clean & Concentrator™-5 were purchased from Zymo Research (Irvine, CA, USA). PureLink RNA Mini Kit was purchased from Invitrogen (Carlsbad, CA, USA). FastStart Universal SYBR Green Master (ROX) was purchased from Roche (Basel, Switzerland). Malonyl-CoA, [$^{13}C_3$] -malonyl-CoA and *p*-coumaric acid, were purchased from Sigma (St. Louis, MO, USA). 4-Hydroxycoumarin was purchased from ACROS ORGANICS (Bridgewater, NJ, USA). Resveratrol was purchased from Tokyo Chemical Industry (Portland, OR, USA). Naringenin was purchased from MP Biomedicals (Santa Ana, CA, USA).

### 2.3.2 Construction of plasmids

For the eGFP assays, to generate eGFP expression plasmids, the e*gfp* gene was PCR-amplified and subcloned into pZE12-luc between Acc651 and XbaI, yielding pZE-eGFP. Likewise, the amplified e*gfp* gene was subcloned into pCS27 and pSA74 between Acc651 and SalI, resulting pCS-eGFP and pSA-eGFP, respectively. The *fabD* gene with its native RBS was PCR-amplified from *E. coli* MG1655 genomic DNA to produce the DNA sequence of *rfabD*. The DNA sequence of the fusion protein FabD/eGFP with *fadD*'s native RBS was generated by SOE-PCR and cloned into pCS27 and pSA74 using BsiWI and BamHI, yielding pCS-RfabD/eGFP and pSA-RfabD/eGFP, respectively. We constructed a parent plasmid pZE-PT. The PT template

consists of two inverted repeat DNA sequences (38 bp) termed PT1 and PT2 with a random DNA sequence between them [34] to facilitate the construction of the plasmids used to produce asRNAs. The random DNA sequence contains two designed restriction sites Acc651 and BamHI to facilitate the insertion of different DNA sequences of asRNAs. The PT template was cloned into the above two plasmids using ApoI and XbaI, yielding pZE-PT and pSA-PT, respectively, to introduce the whole PT template into pZE12-luc and pSA74. The 100, 150, 200 and 300 bp DNA sequences of *egfp* asRNAs were cloned into pZE-PT using Acc651 and BamHI, resulting pZE-aseGFP(100), pZE-aseGFP(150), pZE-aseGFP(200) and pZE-aseGFP(300), respectively, to generate *egfp* asRNA synthesis plasmids. Similarly, plasmids pSA-aseGFP(100), pSA-aseGFP(150), pSA-aseGFP(200) and pSA-aseGFP(300) were generated by using the same cloning strategy. The 100 and 150 bp DNA fragments of *fabD* asRNAs were cloned into pZE-PT using Acc651 and BamHI, resulting pZE-asfabD(100), pZE-asfabD(150), respectively, to generate the *fabD* asRNA synthesis plasmids. Similarly, plasmids pZE-asfabH(100), pZE-asfabH(150), pZE-asfabB(100), pZE-asfabB(150), pZE-asfabF(100) and pZE-asfabF(150) were generated by using the same cloning strategy. The asfabH(100) operon was similarly subcloned into pZE-asfabD(100) using SpeI and SacI, yielding pZE-asfabD(100)-asfabH(100).

For 4-hydroxycoumarin biosynthesis, the DNA fragments *entC-pchB* and *pqsD-sdgA* were amplified from our previous constructed plasmids pZE-EntC-PchB and pCS-PqsD-SdgA [22]. Then the amplified DNA fragments were subcloned into pCS27 to form one operon through three-piece ligation using Acc651, NdeI and XbaI, yielding plasmid pCS-EPPS. For resveratrol biosynthesis, the genes of 4CL2 and STS were cloned into plasmid pCS27 as one operon using Acc651, BglII, and BamHI, generating pCS-STS-4CL. For naringenin biosynthesis, the gene of 4CL2 was cloned into pCS27 using BglII and Acc651, resulting pCS-4CL. Similarly, the genes

of CHI and CHS were cloned as one operon into pCS27 using restriction sites NdeI and BsiWI, yielding pCS-CHI-CHS. The *chi-chs* operon was then subcloned into pCS-4CL using SacI and SpeI, generating pCS-CHI-CHS-4CL.

**Table 2.1** Strains and plasmids used in Chapter 2

| Strain | Genotype | Source |
|---|---|---|
| XL1-blue | *recA1 endA1 gyrA96 thi-1 hsdR17 supE44 relA1 lac [F′ proAB lacI$^q$ZΔM15 Tn10 (Tet$^r$)]* | Stratagene |
| BW25113 | *rrnBT14 ΔlacZWJ16 hsdR514 ΔaraBADAH33 ΔrhaBADLD78* | CGSC |
| **Plasmids** | **Description** | **Reference** |
| pZE12-luc | $P_L$lacO1, *colE* ori, Amp$^r$ | Lutz and Bujard (1997) |
| pCS27 | $P_L$lacO1, *P15A* ori, Kan$^r$ | Shen and Liao (2008) |
| pSA74 | $P_L$lacO1, *pSC101* ori, Cm$^r$ | Huo et al.(2011) |
| pZE-eGFP | pZE12-luc harboring *egfp* | This study |
| pCS-eGFP | pCS27 harboring *egfp* | This study |
| pSA-eGFP | pSA74 harboring *egfp* | This study |
| pZE-PT | pZE12-luc harboring PT template | This study |
| pSA-PT | pSA74 harboring PT template | This study |
| pZE-aseGFP(100) | pZE-PT harboring 100bp aseGFP DNA | This study |
| pZE-aseGFP(150) | pZE-PT harboring 150bp aseGFP DNA | This study |
| pZE-aseGFP(200) | pZE-PT harboring 200bp aseGFP DNA | This study |
| pZE-aseGFP(300) | pZE-PT harboring 300bp aseGFP DNA | This study |
| pSA-aseGFP(100) | pSA-PT harboring 100bp aseGFP DNA | This study |
| pSA-aseGFP(150) | pSA-PT harboring 150bp aseGFP DNA | This study |
| pSA-aseGFP(200) | pSA-PT harboring 200bp aseGFP DNA | This study |
| pSA-aseGFP(300) | pSA-PT harboring 300bp aseGFP DNA | This study |

| | | |
|---|---|---|
| pCS-RfabD/eGFP | pCS27 harboring *fabD* with its native RBS fused with *egfp* | This study |
| pSA-RfabD/eGFP | pSA74 harboring *fabD* with its native RBS fused with *egfp* | This study |
| pZE-asfabD(100) | pZE-PT harboring 100bp as*fabD* DNA | This study |
| pZE-asfabD(150) | pZE-PT harboring 150bp as*fabD* DNA | This study |
| pCS-EPPS | pCS27 harboring *entC, pchB, pqsD* and *sdgA* in one operon | This study |
| pCS-4CL | pCS27 harboring *4cl2* gene from *P. crispum* | This study |
| pCS-STS-4CL | pCS27 harboring *sts* from *V. vinifera* and *4cl2* from *P. crispum* in one operon | This study |
| pCS-CHI-CHS | pCS27 harboring *chi* from *M. sativa* and *chs* from *P. hybrida* in one operon, | This study |
| pCS-CHI-CHS-4CL | pCS27 harboring *chi* from *M. sativa* and *chs* from *P. hybrida* in one operon, and *4cl2* from *P. crispum* in the other operon | This study |
| pZE-asfabH(100) | pZE-PT harboring 100bp as*fabH* DNA | This study |
| pZE-asfabH(150) | pZE-PT harboring 150bp as*fabH* DNA | This study |
| pZE-asfabB(100) | pZE-PT harboring 100bp as*fabB* DNA | This study |
| pZE-asfabB(150) | pZE-PT harboring 150bp as*fabB* DNA | This study |
| pZE-asfabF(100) | pZE-PT harboring 100bp as*fabF* DNA | This study |
| pZE-asfabF(150) | pZE-PT harboring 150bp as*fabF* DNA | This study |
| pZE-asfabD(100)-asfabH(100) | pZE-PT harboring 100bp as*fabD* DNA and 100bp *asfabH* with two operons | This study |

### 2.3.3 Fluorescence Assay

The analysis of interference efficiency was performed by measuring the fluorescence intensity using BioTek micro-plate reader. The transformants of *E. coli* BW25113 containing e*gfp* asRNA synthesis plasmids and eGFP expression plasmids and the transformants containing *fadD* asRNA synthesis plasmids and RFabD-eGFP expression plasmids were cultured in 3.5 ml LB medium with appropriate antibiotics at 37 °C and 290 rpm for 5 h. Then 2% cultures were transferred into baffled flasks containing 15 ml of M9Y media with 1 mM IPTG at 30 °C and 290 rpm. At 6 h, 12 h and 18 h, 1 ml aliquots of cell culture were taken and centrifuged at 10000 rpm, 4 °C for 1 min. The cell pellets were re-suspended in 1 ml of deionized water. Cell cultures (200 µl) were transferred into a black 96-well plate (BRAND plates) and analyzed for eGFP fluorescence intensity using excitation filter of 520 nm, and emission filter of 485 nm. The eGFP fluorescence intensity of each sample was normalized against its $OD_{600}$ and background cell fluorescence was subtracted. Mean values for each sample was obtained from three independent measurements. The reading type was set as endpoint mode [56].

### 2.3.4 Quantitative real-time PCR Analysis

All the transformants of *E. coli* BW25113 containing pZE-PT or pZE-asfabD(100) were cultured in 3.5 ml LB medium with appropriate antibiotics at 37 °C and 290 rpm for 5 h. Then 2% cultures were transferred into baffled flasks containing 15 ml of M9Y media with 1 mM IPTG at 30 °C and 290 rpm. After 12 h, 500 µl cell cultures were taken and centrifuged at 10000 rpm and 4°C for 1 min. The total RNAs were isolated from the above cell pellets using the PureLink RNA Mini Kit. In this process, all the total RNA samples were treated with DNase I to remove the genomic DNA completely. cDNAs were synthesized from 600 ng of heat-denatured

total RNAs using Protoscript II first strand cDNA synthesis kit. qRT-PCR with 12 ng cDNAs was performed using the iQTM SYBR Green Supermix (Bio-Rad) and FastStart Universal SYBR Green Master in 20 µl reaction volume (at least in triplicate) under the following cycling conditions: 95°C for 30 s; 95°C for 10 min; followed by 45 cycles of 95 °C for 15 s; 58 °C for 30 s; 72 °C for 20 s. As a normalizer gene, 16sRNA was amplified with primers (F-5'-GCTCGTGTTGTGAAATGTT, R-5'-TGTAGCCCTGGTCGTAAGG) and the product size was 150 bp. The *fabD* gene fragment was amplified with primers (F-5'-TGAAGAACTGAATAAAACC, R-5'-GCAATAGACGCATCATCCA) and the product size was 274 bp. The specificity of *fabD* primers was confirmed using a BLAST analysis against the NCBI genome database. The integrities of the obtained products were verified by gel electrophoresis on 2% agarose (in 1× TAE buffer) gels. In addition, a melting curve analysis was carried out for each reaction under the following condition: 55°C to 95 °C; 0.5 °C/read; 1 s hold; 72 °C for 10 min. The relative quantification of gene expression between the *E. coli* BW25113 containing plasmid pZE-asfabD(100) and the strain containing plasmid pZE-PT was calculated by the $2^{-\Delta\Delta Ct}$ approximation method [58].

### 2.3.5 Extraction of intracellular malonyl-CoA

All the transformants of *E. coli* BW25113 containing pZE-PT or pZE-asfabD(100) were cultured in 3.5 ml LB medium with appropriate antibiotics at 37 °C and 290 rpm for 5 h. Then 2% cultures were transferred into baffled flasks containing 50 ml of M9Y media with 1 mM IPTG at 30 °C and 290 rpm. After 6 h and 12 h, 20.5 ml and 10.5 ml cell cultures were taken and chilled on ice, respectively. Then the cultures were centrifuged at 6000 rpm and 4°C for 8 min. The supernatants were discarded and the cell pellets were individually re-suspended in 1 ml of

6% perchloric acid (0.125 ml/mg cell) to facilitate cell lysis. Each of the lysed cell suspension was then neutralized with 3 M potassium carbonate (0.3 ml/ml cell lysate). Additionally, 700 ng/ml of [$^{13}C_3$]-malonyl-CoA was spiked into the above mixtures as internal standard and centrifuged at 6000 rpm and 4°C for 8 min. Then, 1.5 ml of supernatant was loaded into a solid-phase extraction column (Sep-Pak C18 Plus Short Cartridge, Waters, WAT020515) pre-conditioned with 2 ml methanol and 2 ml formic acid (pH 3.0), respectively [58, 59]. The loaded column was then washed with 2 ml water and eluted with 1 ml methanol. The eluted samples were dried under a nitrogen stream at 4 °C and dissolved with 150 μl of 0.1% formic acid in 10 mM ammonium acetate/methanol (80:20) for LC/MS/MS [60]. Dry cell weight was calculated according to the empirical rule that 1 $OD_{600}$ = 0.36 g/L [61].

**2.3.6 LC-MS/MS analysis of malonyl-CoA.**

Sample analysis was performed with a LC-MS/MS system using an Agilent 1200 (Agilent Technologies, Santa Clara, CA, USA) separation module connected directly to a Thermo TSQ Ultra triple quadrupole MS system (Thermo Fisher Scientific, San Jose, CA. USA). A 100 × 2.1 mm C18 reverse-phase HPLC column (Thermo Fisher Scientific, San Jose, CA. USA) was used to perform HPLC separation. The analytes were eluted at a flow rate of 250 μl/min with a gradient of 25 mM ammonium acetate (mobile phase A) and 25 mM ammonium acetate in 90% acetonitrile (mobile phase B). Agilent 1200 HPLC binary pump was used to deliver the gradient from 2 to 20 % B over 15 min at a flow rate of 250 μl/min after injecting the samples. The column effluent was directed to Thermo TSQ MS instrument working on ESI positive mode with SRM (selected ion monitor) setting. The instrument was tuned and SRM conditions were optimized by the direct infusion of a solution of standard malonyl-CoA (100 μM) in the ESI ion

source with the same mobile phase used for HPLC separation. The transitions (m/z parent → m/z daughter) for the malonyl-CoA were as follows: (1) malonyl-CoA, 854→347; (2) [$^{13}C_3$]-malonyl-CoA, 857→350. The ratio of measured peak area of malonyl-CoA to the peak area of internal standard ([$^{13}C_3$]-malonyl-CoA) was used for relative quantification.

**2.3.7 HPLC-quantitative analysis.**

Both the standards and samples were quantitatively analyzed by HPLC (Dionex Ultimate 3000) with a reverse-phase ZORBAX SB-C18 column and an Ultimate 3000 Photodiode Array Detector. All the transformants used for the biosynthesis of 4-hydroxycoumarin, resveratrol and naringenin were cultured in 3.5 ml LB medium with appropriate antibiotics at 37°C and 290 rpm for 5 h, then 2% cultures were transferred into baffled flasks containing 15 ml M9Y media with 1 mM IPTG (for resveratrol and naringenin biosynthesis, 1 mM *p*-coumaric acid were added) at 30 °C and 290 rpm. After 24 h, 1 ml cultures were taken to measure $OD_{600}$ values and analyze the products by HPLC.

For the 4-hydroxycoumarin HPLC analysis, solvent A was 0.1% (vol/vol) formic acid in water and solvent B was 100% methanol. The gradient was at a flow rate of 1 ml/min: 20-80% solvent B for 18 min, 80-20% solvent B for 1min and 20% solvent B for additional 4 min. The 4-hydroxycoumarin peak eluted at 11.69 min with this program. For resveratrol and naringenin analysis, solvent A was 0.1% (vol/vol) formic acid in water and solvent B was 100% acetonitrile. The gradient was 30% solvent B for 15 min at a flow rate of 1 ml/min. The resveratrol and naringenin peaks appeared at 4.25 and 8.89 min, respectively. Quantification was based on the peak area in reference to the commercial standards. 4-Hydroxycoumarin and naringenin were detected and quantified by monitoring absorbance at 285 nm. The resveratrol was detected and

quantified by monitoring absorbance at 310 nm. Samples containing over 100 mg/L of products were diluted before running HPLC to maintain a linear concentration–peak area relationship.

## 2.4 Results

### 2.4.1 Development of asRNA tool and characterization of its properties

Sufficient and controllable interference efficiency is a prerequisite for the application of asRNAs in genetic manipulation. Among all the factors that may affect interference efficiency, asRNA stability was primarily taken into consideration. Previous studies have shown that improvement in asRNA stability can lead to enhanced interference efficiency. It has been reported that the stem-loop structure can significantly enhance its stability and increase the asRNA lifetime [35]. In this work, we employed this structure as a scaffold to develop the asRNA tool. We constructed a plasmid carrying two inverted repeat sequences and then inserted the DNA fragment corresponding to the asRNA between them to generate this stem-loop structure. When transcribed into RNA in *E. coli*, the two inverted repeats would complementarily pair with each other and form a double-strand stem structure termed as paired termini (PT); meanwhile the interposed RNA sequence would form the loop (Figure 2.1b). We employed the enhanced green fluorescence protein (eGFP) as a reporter to test the interference efficiency of the above asRNA structure.

The translation initiation region on mRNA covering the ribosome binding site (RBS) and start codon has been reported to be an ideal target for asRNA-mediated gene silencing [34, 62]. In this work, we still selected this target region but further studied the effect of asRNA loop length on interference efficiency. Four asRNAs with various loop lengths (100, 150, 200 and 300 nt) complementary to eGFP mRNA were selected, all of which initiate from the -20 nt upstream the

RBS. Initially, we employed a high-copy-number (50-70) plasmid pZE-aseGFP for asRNA generation, and a low-copy-number (10-12) plasmid pSA-eGFP for the reporter eGFP expression. When the two plasmids were co-transferred into *E. coli*, the asRNAs with different lengths exhibited varied interference efficiencies. The construct with a 100-nt loop decreased the eGFP fluorescence intensity by about 80% during 6-24 h, compared with the RNA scaffold without the loop; while the interference efficiencies of the asRNAs with 150-, 200- and 300-nt loops were 44, 50 and 38 % on average, respectively (Figure 2.2). These results suggested that longer asRNA sequences do not necessarily lead to higher interference efficiencies. In addition, we observed that the interference efficiencies at 3 h were slightly higher than those after 6 h for all loop lengths.

Furthermore, we also examined the effect of the relative abundance between asRNAs and their target mRNAs on the interference efficiencies. When we continued using the high-copy-number plasmid for asRNA generation, but employed a medium-copy-number (20-30) plasmid pCS-eGFP instead of the low-copy-number plasmid to express the reporter eGFP, the interference efficiency of the 100-nt asRNA decreased from 80% to 65%; while no significant change in interference efficiency was observed for other lengths. Interestingly, when we used a low-copy-number plasmid (10-12) pSA-aseGFP for asRNA synthesis but a high-copy-number plasmid for eGFP expression, the interference efficiencies for all the asRNAs fell below 20%. These results indicated that high abundance of asRNAs relative to their target mRNAs is critical to achieve high interference efficiency. It is also reasonable to conclude that asRNAs generated with high-copy-number plasmids should be more efficient in down-regulating the expression of chromosomal genes.

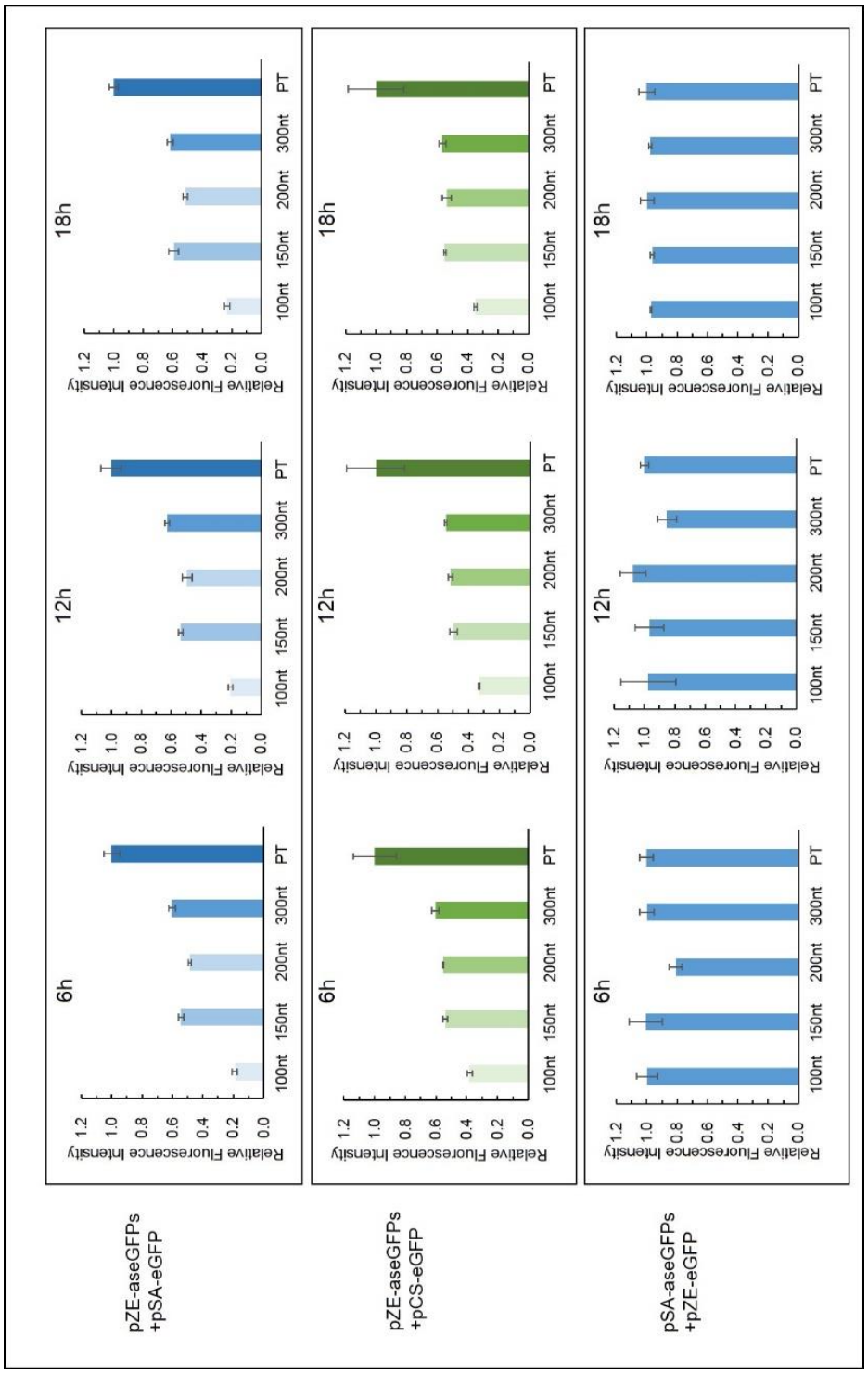


**Figure 2.2** Interference efficiencies of asRNAs with varied loop lengths and relative abundance. (a) eGFP expression (low copy) interfered by asRNAs (high copy) with 100, 150, 200 and 300-nt

loop lengths. (b) eGFP expression (medium copy) interfered by asRNAs (high copy). (c) eGFP expression (high copy) interfered by asRNAs (low copy). We set the relative fluorescence intensity of the negative control strains carrying pZE-PT or pSA-PT as 1.0 (or 100%) for each time point. Interference efficiency (%) = 100% – relative fluorescence intensity. All the data points were normalized by their respective $OD_{600}$ values. The results were generated from three independent experiments.

### 2.4.2 Design and characterization of asRNAs targeting *fabD*

In the fatty acid biosynthesis, several genes, such as *fabD, fabF* and *fabB* are involved in malonyl-CoA consumption. Particularly, the malonyl-CoA: ACP transacylase encoded by *fabD* is the first step for malonyl-CoA consumption, leading to the generation of malonyl-ACP. Previous studies have reported that the genetic inactivation of gene *fabD* was lethal for cells [28]. In this study, we first targeted this gene to demonstrate the effectiveness of asRNAs on the repression of fatty acid biosynthesis and enrichment of cellular malonyl-CoA. However, to facilitate the measurement of *fabD* interference, we constructed a FabD/eGFP fusion protein, which can indicate the expression level of gene *fabD* through fluorescence signal monitoring. We introduced the native RBS of *fabD* upstream the FabD/eGFP gene and cloned them into a low-copy-number plasmid pSA74, yielding pSA-RfabD/eGFP to better simulate the expression of chromosomal genes. However, the FabD/eGFP fusion protein expressed by this low-copy plasmid showed very weak fluorescence signal, which was inconvenient for measurement due to the sensitivity limit of the detection device. Thus, we shifted to a medium-copy plasmid pCS-RfabD/eGFP for expressing the fusion protein instead of pSA-RfabD/eGFP (Figure 2.3a). Meanwhile, we designed *asfabD* targeting the RBS and coding region of *fabD* mRNA and

generate it with a high copy number plasmid pZE-asfabD(100). When pZE-asfabD(100) and pCS-RfabD/eGFP were co-transferred into *E. coli*, the green fluorescence intensity decreased by 58.8% (Figure 2.3b) compared with the control strain carrying pZE-PT and pCS-RfabD/eGFP, indicating that the developed asRNA tool is applicable for the *fabD* interference.

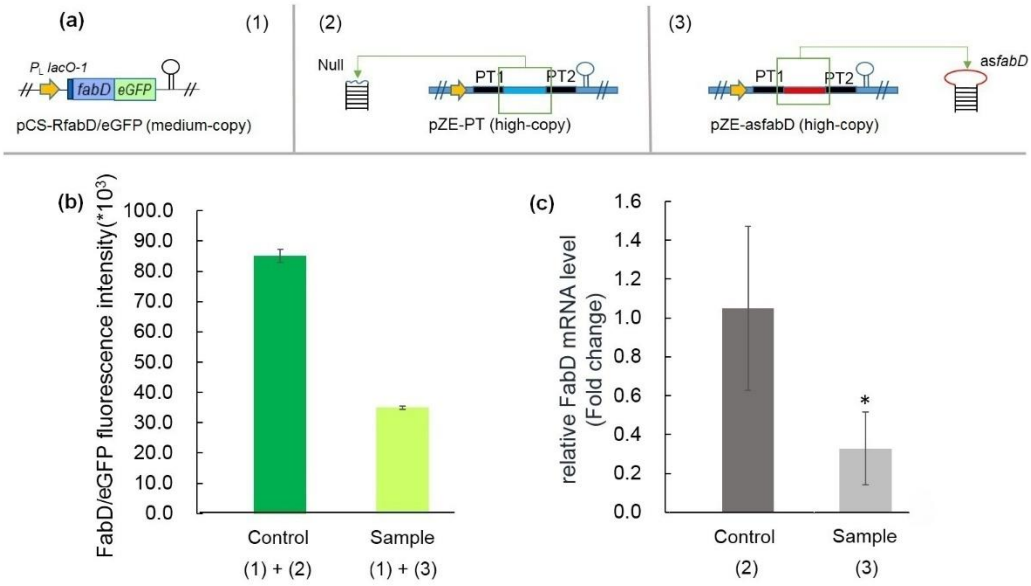


**Figure 2.3** Effects of the *fabD* asRNA at translational and post-transcriptional levels. (a) Schematic representation of plasmid construction. (1) FabD/eGFP fusion protein expressed by a medium-copy-number plasmid. (2) Negative control plasmid only containing the stem structure (PT sequences) without asRNA loop. (3) asRNA generating plasmid containing the *fabD* asRNA with a 100-nt loop; (b) Fluorescence intensity of FabD/eGFP fusion protein interfered by as*fabD*(100). The results were generated from three independent experiments; (c) Relative mRNA level of gene *fabD* in *E. coli* strains. For the negative controls, three different transformants were used; for the samples, five different transformants were used. For each transformant, qRT-PCR was repeated for three times. For each transcript of gene *fabD* in all

samples and negative controls, the values are normalized to the internal control (16srRNA). *: p = 0.04 was analyzed by unpaired, one-tailed Student's t test.

### 2.4.3 The effect of as*fab*D interference at transcriptional and metabolite level

Previous studies indicated that asRNA may not only function at the translational level, but also repress gene transcription or trigger mRNA degradation [63]. We introduced pZE-asfabD(100) into wild-type *E .coli* and performed real-time PCR to detect the variation of the *fabD* mRNA level to verify whether the *fabD* expression was interfered before translation. As shown in Figure 2.3c, the relative mRNA levels of gene *fabD* (from five transformants) were remarkably reduced at 12 h, compared with those of the control strain carrying pZE-PT, (from three transformants), indicating that the as*fabD* can cause the decrease of intracellular *fabD* mRNA abundance. We detected malonyl-CoA concentration by LC-MS/MS to further investigate whether the down-regulated expression of gene *fabD* can result in the enrichment of cellular malonyl-CoA. As shown in Figure 2.4, the engineered strain carrying pZE-asfabD(100) showed 4.37 and 4.52-fold increases in malonyl-CoA concentration at 6 h and 12 h, respectively, compared with the control strain with pZE-PT. The results above clearly demonstrate that asRNA-mediated down-regulation of *fabD* gene expression occurred at post-transcriptional and translational level, the overall effect of which is the repression of fatty acid biosynthesis and the enrichment of malonyl-CoA.

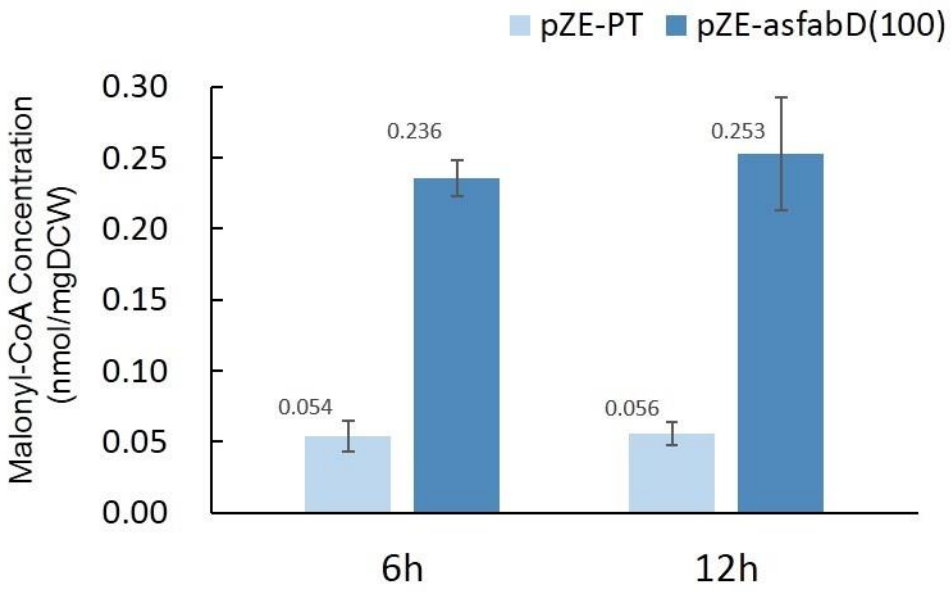


**Figure 2.4** Intracellular concentrations of malonyl-CoA. Light blue: strain expressing null asRNAs (negative control). Dark blue: the strain expressing *fabD* asRNA with a 100-nt loop. DCW: dry cell weight. The results were generated from three independent experiments.

### 2.4.4 Production enhancement of malonyl-CoA derived molecules by *asfabD* interference

We firstly used the biosynthesis of 4-hydroxycoumarin, a pathway well established in our previous work [22], as a demonstration to examine if the enriched malonyl-CoA pool can be redirected into desired pathways. Four pathway genes encoding EntC, PfPchB, PqsD and SdgA were consecutively cloned as an operon in a medium-copy-number plasmid pCS-EPPS (Figure 2.5a). When pCS-EPPS and pZE-asfabD(100) were simultaneously introduced into *E. coli* BW25113, the resulting strain produced 270.85 mg/L of 4-hydroxycoumarin at 24 h. In contrast, the control strain BW25113 carrying pCS-EPPS and pZE-PT (a backbone plasmid without asRNA loop) was only able to produce 106.95 mg/L 4-hydroxycoumarin, indicating that inhibition of *fabD* expression by asRNA led to a 2.53-fold increase in the 4-hydroxycoumarin

titer (Figure 2.5b). In addition, we observed that the *fabD* down-regulated strain did not show obvious growth retardation (Table 2.2).

Two other established pathways leading to the biosynthesis of model polyketides resveratrol and naringenin were also tested to further verify the effect of the down-regulated *fabD* expression on the production of other malonyl-CoA derived molecules. Previous studies reported that over-expression of 4-coumarate:CoA ligase (4CL) and stilbene synthesis (STS) in *E. coli* led to the production of resveratrol from *p*-coumaric acid; while the production of naringenin requires the expression of 4CL, chalcone synthase (CHS) and chalcone isomerase (CHI) [20, 21]. Therefore, we constructed two plasmids pCS-STS-4CL and pCS-CHI-CHS-4CL to express the genes involved in resveratrol and naringenin biosynthesis, respectively. When these two plasmids were separately co-transferred with the control plasmid pZE-PT into *E. coli*, the titers of resveratrol and naringenin achieved 158.22 and 59.58 mg/L, respectively. In contrast, when the pCS-STS-4CL was co-transformed with pZE-asfabD(100), the resveratrol titers achieved 268.20 mg/L, a 1.70-fold increase compared with the control strain (Figure 2.5c); while naringenin titer for the strain carrying pCS-CHI-CHS-4CL and pZE-asfabD(100) was 91.31 mg/L, representing a 1.53-fold improvement (Figure 2.5d). All the significant titer improvements for these three heterologous products demonstrate that asRNAs have been developed as a powerful tool to inhibit essential genes.

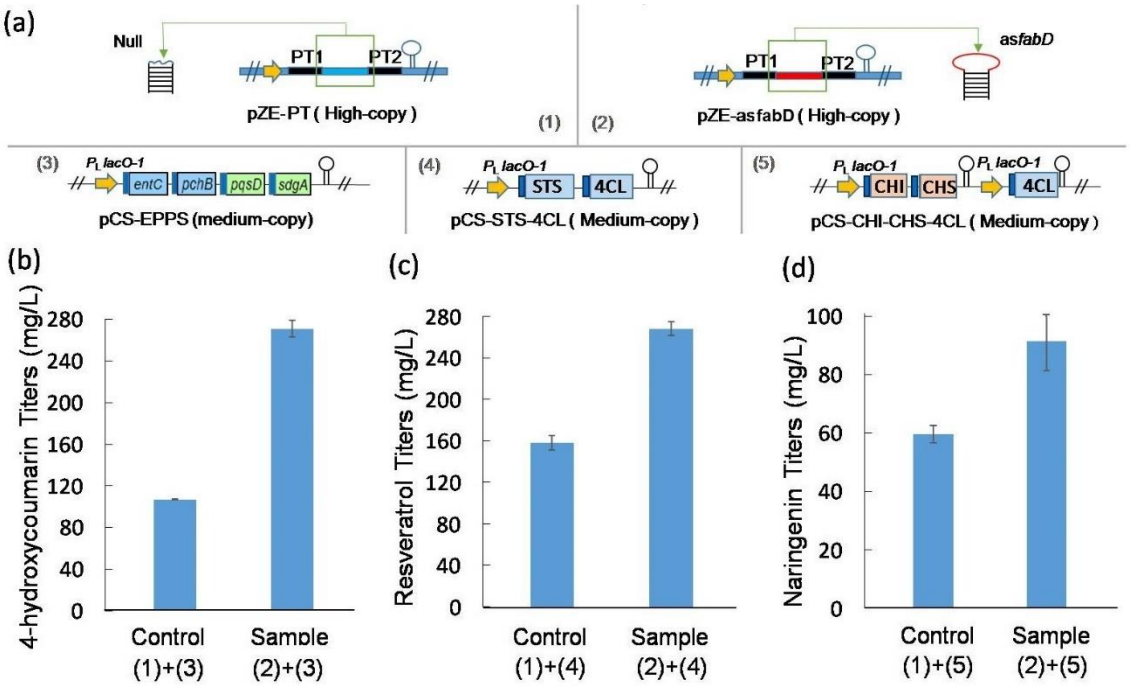


**Figure 2.5** Heterologous production of malonyl-CoA derived compounds with and without the effects of asRNAs. (a) Schematic representation of plasmid construction. (1) Negative control plasmid. (2) asRNA generating plasmid. (3) The plasmid carrying 4-hydroxycoumarin biosynthetic genes. (4) The plasmid carrying resveratrol biosynthetic genes. (5) The plasmid carrying naringenin biosynthetic genes. (b) 4-hydroxycoumarin titers; (c) resveratrol titers; (d) naringenin titers. The results were generated from three independent experiments.

### 2.4.5 Effects of other down-regulated *fab* genes on 4-HC pathway

In addition to *fabD*, we also examined the effect of the down-regulation of other *fab* genes including *fabB* and *fabF* and *fabH* on 4-HC biosynthesis. As shown in the Figure 1a, β-oxoacyl-ACP synthase I (KAS I) encoded by gene *fabB* catalyze the repeated condensation of malonyl-ACP to form β-oxoacyl-ACP; while KAS II encoded by *fabF* is an isoenzyme of KAS I, which is also responsible for the elongation of fatty acid chains [64, 65]. Since both of these consume the intermediate downstream of malonyl-CoA, we further selected these two targets for asRNA

interference study. Using similar approaches, we constructed two plasmids pZE-asfabB(100) and pZE-asfabF(100) to generate the asRNAs with 100-nt loops targeting *fabB* and *fabF*, respectively. When pZE-asfabB(100) and pZE-asfabF(100) were separately transferred with pCS-EPPS carrying 4-hydroxycoumarin biosynthetic genes into *E. coli*, as shown in Table 2.2, 4-hydroxycoumarin was produced at the titers of 116.95 and 173.66 mg/L, representing a 1.09-fold and a 1.62-fold increase, respectively, compared with the control strain without asRNA interference (106.95 mg/L, see section 2.3.4). Apparently, the repression of *fabB* and *fabF* is not as efficient as that of *fabD*. However, we observed that the *fabB* and *fabF*-interfered strains showed obvious growth retardation compared with the *fabD*-interfered strain during the early stage of cultivation (data not shown). We speculated that the interference efficiency of the asRNAs with 100-nt loops might be excessively high for *fabB* and *fabF* repression, which is harmful to normal cell growth. We employed weaker asRNAs with 150-nt instead of 100-nt lengths to verify this hypothesis. As shown in Table 2.2, the strains with *fabB* and *fabF* interfered by the asRNAs with 150-nt loops showed a 1.79-fold and a 2.49-fold increase in 4-hydroxycoumarin titers, respectively, much higher than those by the asRNAs with 100-nt loops. In addition, 3-ketoacyl-ACP synthase III encoded by *fabH* was also tested. Employment of the asRNAs with 100 and 150-nt loops led to a 1.86-fold and a 2.12-fold increase in 4-hydroxycoumarin production, respectively, showing a similar trend to *fabB* and *fabF* interference. Based on these results, we conclude that high interference efficiency on the fatty acid biosynthesis is not always beneficial for the production of malonyl-CoA derived compounds. Balanced allocation of malonyl-CoA between cell growth and heterologous molecules production is desirable to prevent the impairment of cell viability.

**Table 2.2** Effect of down-regulated *fab* genes on 4-hydroxycoumarin production

| **Negative Control** | **$OD_{600}$** | **4-HC Titers(mg/L)** | **Fold** |
|---|---|---|---|
| pZE-PT + pCS-EPPS | 9.33 ± 0.11 | 106.95 ± 0.13 | 1.00 |
| **Loop size = 100nt** | **$OD_{600}$** | **4-HC Titers(mg/L)** | **Fold** |
| pZE-asfabH + pCS-EPPS | 8.71 ± 0.13 | 199.43 ± 9.78 | 1.86 |
| pZE-asfabF + pCS-EPPS | 8.01 ± 0.88 | 173.66 ± 10.86 | 1.62 |
| pZE-asfabB + pCS-EPPS | 8.74 ± 0.29 | 116.95 ± 15.90 | 1.09 |
| pZE-asfabD + pCS-EPPS | 9.34 ± 0.96 | 270.85 ± 7.85 | 2.53 |
| pZE-asfabD-asfabH + pCS-EPPS | 8.71 ± 0.13 | 235.22 ± 7.25 | 2.20 |
| **Loop size = 150nt** | **$OD_{600}$** | **4-HC Titers(mg/L)** | **Fold** |
| pZE-asfabH + pCS-EPPS | 10.02 ± 0.05 | 226.23 ± 1.99 | 2.12 |
| pZE-asfabF + pCS-EPPS | 8.63 ± 0.07 | 266.41 ± 7.00 | 2.49 |
| pZE-asfabB + pCS-EPPS | 8.78 ± 0.29 | 191.91 ± 20.5 | 1.79 |
| pZE-asfabD + pCS-EPPS | 8.14 ± 0.18 | 212.34 ± 7.36 | 1.99 |

All data are reported as mean ± s.d. from three independent experiments.

In addition to targeting single genes, we also explored the simultaneous interference of two genes by asRNAs to investigate whether the effect of malonyl-CoA enrichment can be accumulated. As shown in Table 2.2, interferences of single genes *fabD* and *fabH* by the asRNAs with 100-nt loops are among the most efficient ones in improving 4-hydroxycoumarin production. Therefore, we constructed a plasmid pZE-asfabD(100)-asfabH(100) to generate the asRNAs with 100-nt loops targeting *fabD* and *fabH* simultaneously. When it was transferred into *E. coli* together with pCS-EPPS, we observed a 2.20-fold increase in 4-hydroxycoumarin production compared with the control strain without asRNA interference, which is slightly lower than the strain with only *fabD* interfered (2.53-fold). These results suggested that *fabD* is the most desired target to inhibit the malonyl-CoA consumption. Additional interference of other *fab* genes may not further improve the titers of malonyl-CoA derived compounds significantly.

## 2.5 Discussion

Gene knock-out strategy has been playing a significant role in charactering gene functions or engineering cells for desirable metabolic properties [66]. However, this strategy is usually limited to those genes that are not essential for cell growth. Alternatively, asRNA has been exploited to overcome this limitation by conditionally down-regulating the expression of essential target genes. Through binding to the translation initiation region (e.g. RBS and start codon) of target mRNA, a reversible steric effect leads to a knockdown regulation by blocking the ribosome reading through mRNA and inhibiting the translation of the corresponding genes [68]. This property promoted us to investigate the factors critical for interference efficiency and strategies to control the efficiency.

In this study, we employed an artificial stem-loop structure to improve the stability of asRNA, then optimized its loop size to achieve the fine-tuning of its interference efficiency. We observed from the results that shorter asRNAs exhibited higher interference efficiency within the range of 100-300 nt. We speculated that the longer loops might form more complicated secondary structures that weaken their binding to target mRNAs or decrease the asRNA stability. Additionally, we observed that higher relative abundance of asRNA over its target gene was critical to achieve high interference efficiency (Figure 2.2). Based on the generalized rules, we applied asRNAs to interfere fatty acid biosynthesis genes. We evaluated its interference efficiency and demonstrated its effect at transcriptional, translational and metabolic levels through real-time PCR, eGFP fusion protein reporter and LC/MS/MS, respectively. In practice, the single interference of *fabD* led to a 4.52-fold increase in intracellular malonyl-CoA concentration, demonstrating the effectiveness of the *fabD* asRNA. Then, we introduced the designed *fabD* asRNA into three heterologous pathways of malonyl-CoA derived natural

products and achieved 2.53-fold, 1.70-fold and 1.53-fold increases in 4-hydroxycoumarin, resveratrol and naringenin production, respectively. Apparently, the titers of these compounds were not increased as much as the level of malonyl-CoA, which may be explained by the following two reasons. On one hand, the enriched malonyl-CoA might have saturated the heterologous enzymes; on the other hand, these pathways involve other precursors (e.g. salicoyl-CoA and *p*-coumaroyl-CoA), which may also be determinative factors for production.

We used the biosynthesis of 4-hydroxycoumarin as a model system, and targeted other genes directly and/or indirectly related to malonyl-CoA consumption with asRNAs to further investigate this strategy. As shown in Table 2.2, in addition to gene *fabD*, interference of other genes such as *fabB, fabF* and *fabH* also led to significant improvements in 4-hydroxycoumarin production. However, the interference efficiency has varied effects on the different *fab* genes. For example, the interference of gene *fabD* with the asRNAs with 100 and 150-nt loops showed similar results; while for *fabB, fabF* and *fabH,* the asRNAs with 150-nt loops were obviously advantageous than the asRNAs with 100-nt loops. Meanwhile, we observed growth retardation for strains with genes *fabB, fabF* and *fabH* interfered by the asRNAs with 100-nt loops, indicating that excessively strong inhibition of these genes may impair cell viability. Based on the analysis above, we conclude that high interference efficiency is not always necessary to achieve high titers. A balanced allocation of malonyl-CoA between necessary cell growth and heterologous production is critical to maintain the desired viability of the microbial cell factories and achieve the most efficient production. Therefore, asRNA design and interference efficiency should be further investigated to provide more controllable tools for metabolic engineering use. As we were preparing this manuscript, the use of antisense RNA strategy to enhance the production of naringenin was reported [68]. Compared with this work which focused on a single

target product, we have demonstrated that regulating malonyl-CoA using antisense RNA can be a platform technology for improving the production of a variety of molecules (e.g. 4-HC, resveratrol and naringenin) derived from malonyl-CoA. In addition, we conducted a more systematic study on the effect of down-regulating several fatty acid biosynthesis genes on the enrichment of intercellular malonyl-CoA. Overall, this work demonstrates that antisense RNA is a promising genetic tool to increase microbial production of economically and pharmaceutically valued compounds.

# CHAPTER 3[1]

## ANTISENSE RNA ELEMENTS FOR DOWNREGULATING EXPRESSION

[1] Yaping Yang, Jian Wang, Ruihua Zhang, Yajun Yan. 2015. Submitted to Methods in Molecular Biology, 12/30/16.

## 3.1 Abstract

Antisense RNA (asRNA) technology is an important tool for downregulating gene expression. When applying this strategy, the asRNA interference efficiency is determined by several elements including scaffold design, loop size, and relative abundance. Here, we take the *Escherichia coli* gene *fabD* encoding malonyl-CoA-[acyl-carrier-protein] transacylase as an example to describe the asRNA design with reliable and controllable interference efficiency. Real-time PCR and fluorescence assay methods are introduced to detect the interference efficiency at RNA level and protein level, respectively.



**Keywords** asRNA, scaffold design, loop size, relative abundance, interference efficiency detection, gene *fabD*


## 3.2 Introduction

Antisense RNA (asRNA) mediated gene silencing has been extensively utilized as a critical tool to control gene expression without any genomic modification of the target gene [68-70]. Through base pairing between designed asRNA and target mRNA, the resulting double strand RNA (dsRNA) can inhibit translation initiation by steric hindrance and trigger degradation of the target mRNA by dsRNA-specific RNases (*see* Figure 3.1(c)) [40,71,72]. There are advantages of employing the asRNA strategy. Unlike the traditional gene knockout strategy for disrupting gene expression, the asRNA triggered gene downregulation still maintains the cell viability. The plasmids for asRNA expression can be easily constructed, conditionally controlled by various promoters, and designed to target several genes simultaneously. However, the asRNA-mediated gene inhibition requires continuous presence of abundant asRNA molecules. Thus, the reliable supply and stability of asRNA are prerequisite for this strategy to be applied efficiently in genetic

manipulations. The asRNA interference efficiency is mainly affected by several factors, among which asRNA stability is the primary player [73, 74]. Previous reports have shown that asRNA scaffold was beneficial to asRNA stability, like Hfq protein-assisted asRNA scaffold showed an increased lifetime and effectiveness in target binding [44,75]. A stem-loop asRNA scaffold also exhibited a prolonged half-life and efficient target recognition without the involvement of any protein [35] (*see* Figure 3.1). For this stem-loop scaffold, two 38 bp inverted repeats were the essential parts to maintain the asRNA stability [66] (*see* Figure 3.1(b)). Herein, we create an efficient method to assemble the basic stem-loop scaffold with a random DNA fragment. By replacing the random DNA fragment with a specific sequence complementary to the translation initiation region of any target gene, various new artificial regulatory asRNAs would be created [16]. Another strategy to improve asRNA interference efficiency is to optimize the asRNA loop size. Our previous work reported that interference efficiency was negatively correlated with the asRNA loop size and asRNA with 100-nt loop length conducted up to 80 % interference efficiency [16]. To simplify the experimental operation as well as to ensure high interference efficiency, we recommend 100-nt as the primary choice for the asRNA loop design [16]. Finally, the relative asRNA abundance is crucial to enhance interference efficiency [35, 76]. The excess intracellular asRNAs enable an efficient competition over ribosome to sequester target mRNAs. Thus, we recommend constructing asRNAs on the high copy number plasmid or under control of strong promoters. real-time quantitative PCR and eGFP fluorescence assay are performed to detect the interference efficiency at RNA level and protein level. Here, by taking *Escherichia coli* malonyl-CoA-[acyl-carrier-protein] transacylase gene *fabD* as an example, we demonstrate the asRNA design with reliable and controllable interference efficiency.

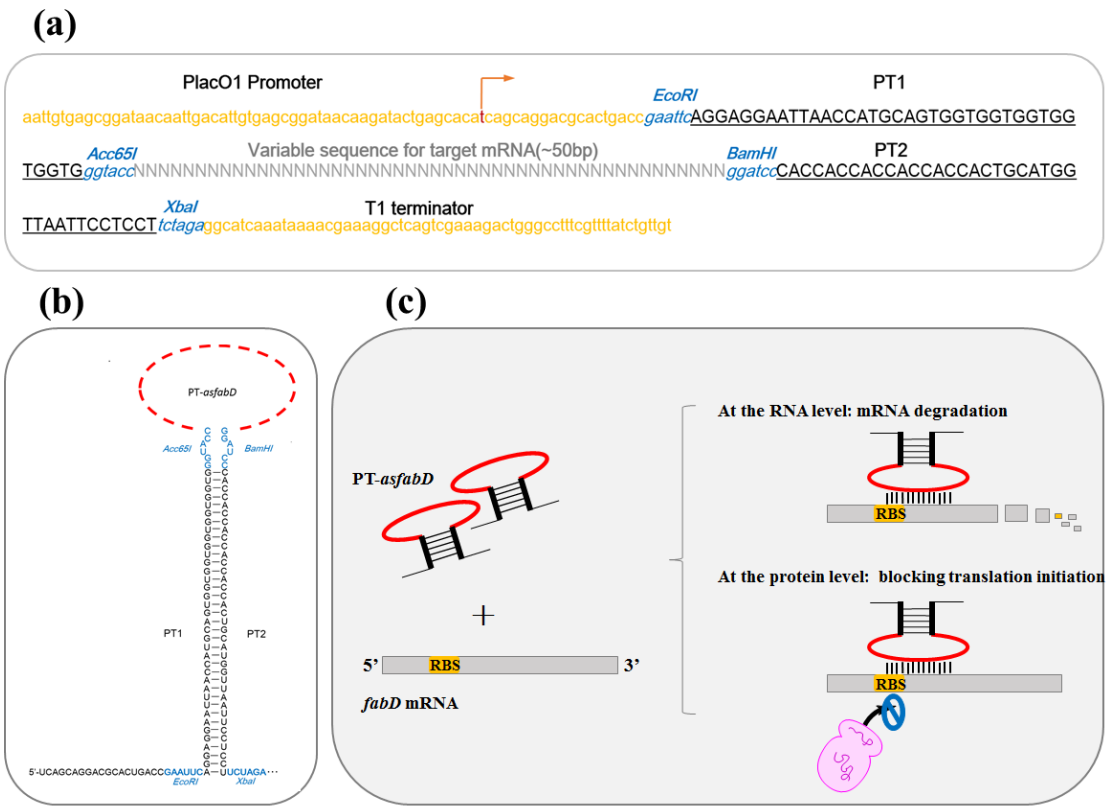


**Figure 3.1** The stem-loop scaffold and asRNA interference mechanism. (a) The DNA sequence of two 38 bp inverted repeats. (b) *asfabD* scaffold. When *asfabD* is transcribed in *E. coli*, the two PT would complementarily pair with each other and generate a double-strand stem structure, meanwhile the interposed *asfabD* sequence would form the loop. (c) asRNA interference mechanism. When asRNA complementarily binds to target mRNA, the resulting double strand RNA (dsRNA) will trigger degradation of the target mRNA or block translation initiation by steric hindrance.

### 3.3 Materials

Prepare all solutions by deionized water (di$H_2O$) and analytical grade reagents. Autoclave all solutions at 121 ℃ for 20 min. Prepare and store all reagents at room temperature (unless specified otherwise).

3.3.1 Construction of asRNA interference plasmids

1. Backbone plasmids: high copy number plasmid pZE12-luc and low copy number plasmid pSA74.
2. Polymerase chain reaction (PCR): Genomic DNA of *E. coli* BW25113, primers (*see* Table 3.1), Phusion High-Fidelity DNA polymerase, 10×buffer, DMSO (if necessary)
3. Restriction endonucleases: *EcoR*I, *Acc65*I, *BamH*I, *Xba*I, *Sph*I, *Spe*I..
4. Tris-acetate-EDTA (TAE) Buffer (50×): 242 g Tris free base, 18.61 g disodium EDTA, 57.1 ml glacial acetic acid and di$H_2O$ to a final volume of 1 liter.
5. 0.8 % agarose gel: 0.8 g agarose in 100 ml TAE buffer.
6. DNA ladder: Generuler 1kb DNA ladder.
7. All kits for gene cloning: PCR purification kit, Gel DNA recovery kit, Quick ligation kit, Plasmid miniprep kit.
8. Competent cells: *E. coli* XL-Blue and BW25113.
9. LB medium: 10 g tryptone, 5 g yeast extract and 10 g NaCl in di$H_2O$ to a final volume of 1 liter.
10. Agar plates: each 9 cm diagram petri dish contains 10 ml LB medium containing 1.5 % agar.
11. Antibiotics: ampicillin (100 mg/L), chloramphenicol (34 mg/L)

3.3.2 Fluorescence Assay

1. eGFP cDNA.
2. Inducer: 0.5 M isopropyl β-D-1-thiogalactopyranoside (*IPTG*).
3. Black 96-well plate with clear bottom.
4. BioTek plate reader.

**Table 3.1** Primer sequences for cloning and Qrt-PCR analysis in chapter 3

| Primers | Primer Sequence (5'-3') |
|---|---|
| 1 | AAAAAgaattcAggaggaaTTaaccaTgcagTggTggTggTggTggTgGGTACCgatatc |
| 2 | aaaaaGcatgccatggcggccgcaagcttgatatcGGTACCcAccAccAccAccAccAc |
| 3 | AAAAAgcatgCgatatcaagcttgcggccgccatggatccCaccaccaccaccaccacTg |
| 4 | AAAAAtctagaAggAggAAttAAccAtgcAgtggtggtggtggtggtGggatccatggcg |
| 5 | AAAAAGGTACCCCGCCATATCAGCCAGCATTCCAAC |
| 6 | AAAAAGGATCCAGTTGGTTCTGCTTGAAGCCTTTGG |
| 7 | GCTCGTGTTGTGAAATGTT |
| 8 | TGTAGCCCTGGTCGTAAGG |
| 9 | TGAAGAACTGAATAAAACC |
| 10 | GCAATAGACGCATCATCCA |
| 11 | aaaaaggtaccAACTCGGTATGTCTATGGATAATGTC |
| 12 | ACAGCTCCTCGCCCTTGCTCACAAGCTCGAGCGCCGCTGCCATC |
| 13 | GATGGCAGCGGCGCTCGAGCTTGTGAGCAAGGGCGAGGAGCTGT |
| 14 | aaaaaggatccTTACTTGTACAGCTCGTCCATGCCGAG |

3.3.2.1 Quantitative real-time (qRT) PCR Analysis

All materials should be RNase-free in this section. All solutions are prepared by RNase-free water and containers.

1. Total RNA isolation: RNA purification kit, RNase-free pipette tips, RNase free water, 1.5 ml RNase-free microcentrifuge tubes, micro tube homogenizer system, DNase I, 2-mercaptoethanol, 100 % ethanol, 10 % SDS (0.5 μl/sample), Lysozyme solution (100 μl/sample): 10 mM Tris-HCL (pH 8.0), 0.1 mM EDTA, 10 mg/ml lysozyme, Lysis buffer: before beginning of the lysis and homogenization steps, prepare a fresh amount of lysis buffer (10 μl 2-mercaptoethanol/1 ml lysis buffer). Use 350 μl fresh lysis buffer for 1 ×

$10^9$ bacterial cells.

1. The cDNA synthesis: Primers (*see* Table 3.1), Protoscript II first strand cDNA synthesis kit, sterile aerosol pipet tips, RNase free water.
2. qRT-PCR: primers (*see* Table 3.1), FastStart Universal SYBR Green Master, 8 strip tube.
3. The required equipment: NanoDrop 2000c UV-Vis Spectrophotometer, iQTM SYBR Green Supermix.
4. M9Y medium: 10 g glucose, 6 g $Na_2HPO_4$, 0.5 g NaCl, 3 g $KH_2PO_4$, 1 g $NH_4Cl$, 1 mM $MgSO_4$ (final concentration), 0.1 mM $CaCl_2$ (final concentration), 2 g yeast extract, 2 g sodium citrate, and 100 mg serine dissolved in di$H_2O$ with a final volume of 1 liter.

## 3.4 Methods

### 3.4.1 Construction of the stem-loop scaffold carrying asRNA

3.4.1.1 Construct parent plasmid pZE-PT (*see* Figure 3.2, Note 3.5.1):

1. Amplify the DNA fragment 1 by PCR reaction. Dilute primer 1 and 2 using di$H_2O$ to 1 μM. Prepare the PCR mixture (50 μl) using Phusion High-Fidelity DNA polymerase as following: di$H_2O$: 30.5 μl, 10×buffer: 10 μl, 2 mM dNTP: 5 μl, primer 1&2: 2 μl (each), Enzyme: 0.5 μl. During this mixture, primer 1 and 2 serve as both primers and template. The PCR product of DNA fragment 1 is 85 bp (*see* Note 3.5.2). The PCR program is: pre-denaturation at 98 ℃ for 3 min, 30 cycles of 98 ℃ for 30 sec, 60 ℃ for 30 sec and 72 ℃ for 20 sec, then extension at 72 ℃ for another 5 min, followed by cooling down to 16 ℃.

2. Amplify the DNA fragment 2 by PCR reaction using primer 3 and 4. The procedures are the same as 3.4.1.1.1. The PCR product of DNA fragment 2 is 85 bp (*see* Note 3.5.2).

3. Purify DNA fragment 1 and 2 using PCR purification kit. Add 100 µl binding buffer into each 50 µl DNA fragment. Mixed by pipette. Transfer the mixture into a spin column with a collection tube. After 1 min, centrifuge the spin column at 8,000 rpm for 1 min. Add 200 µl wash buffer into the spin column. Then centrifuge at 12,000 rpm for 30 sec. Transfer column to a 1.5 ml centrifuge tube. After 1 min, add 30 µl di$H_2O$ to elute the DNA from the spin column (*see* Note 3.5.3).

4. Prepare a mixture of enzyme digestion as following. For DNA fragment 1 and 2: di$H_2O$: 17 µl, DNA: 15 µl, 10×buffer: 4 µl, enzymes (*see* Note 3.5.4): 2 µl (each), total volume: 40 µl. For plasmid pZE-luc: di$H_2O$: 26 µl, DNA: 6 µl, Buffer: 4 µl, Enzymes (*see* Note 3.5.4): 2 µl (each), total volume: 40 µl. Incubate the digested mixture at 37 ℃ for 2-4 hrs in a water bath.

5. Purify the digested products. For DNA fragment 1 and 2: we use the same method as 3.4.1.1.3 and 6 µl di$H_2O$ is added for elution. For plasmid pZE-luc: load digested product into a 0.8 % agarose gel. Run the gel in the 1×TAE buffer using 100 constant voltage for 20 min. Observe the gel under low UV. Cut the gel containing target fragment, and place it in a centrifuge tube and purified the DNA using gel DNA recovery kit. Add ADB buffer (300 µl/100 mg, the volume of buffer over the weight
of agarose) into the centrifuge tube. Melt the gel at 55 ℃ for 5 min in a water bath. After the gel completely melts, place it in a spin column with a collection tube. The next step is the same as 3.4.1.1.3. But we add 6 µl di$H_2O$ for elution.

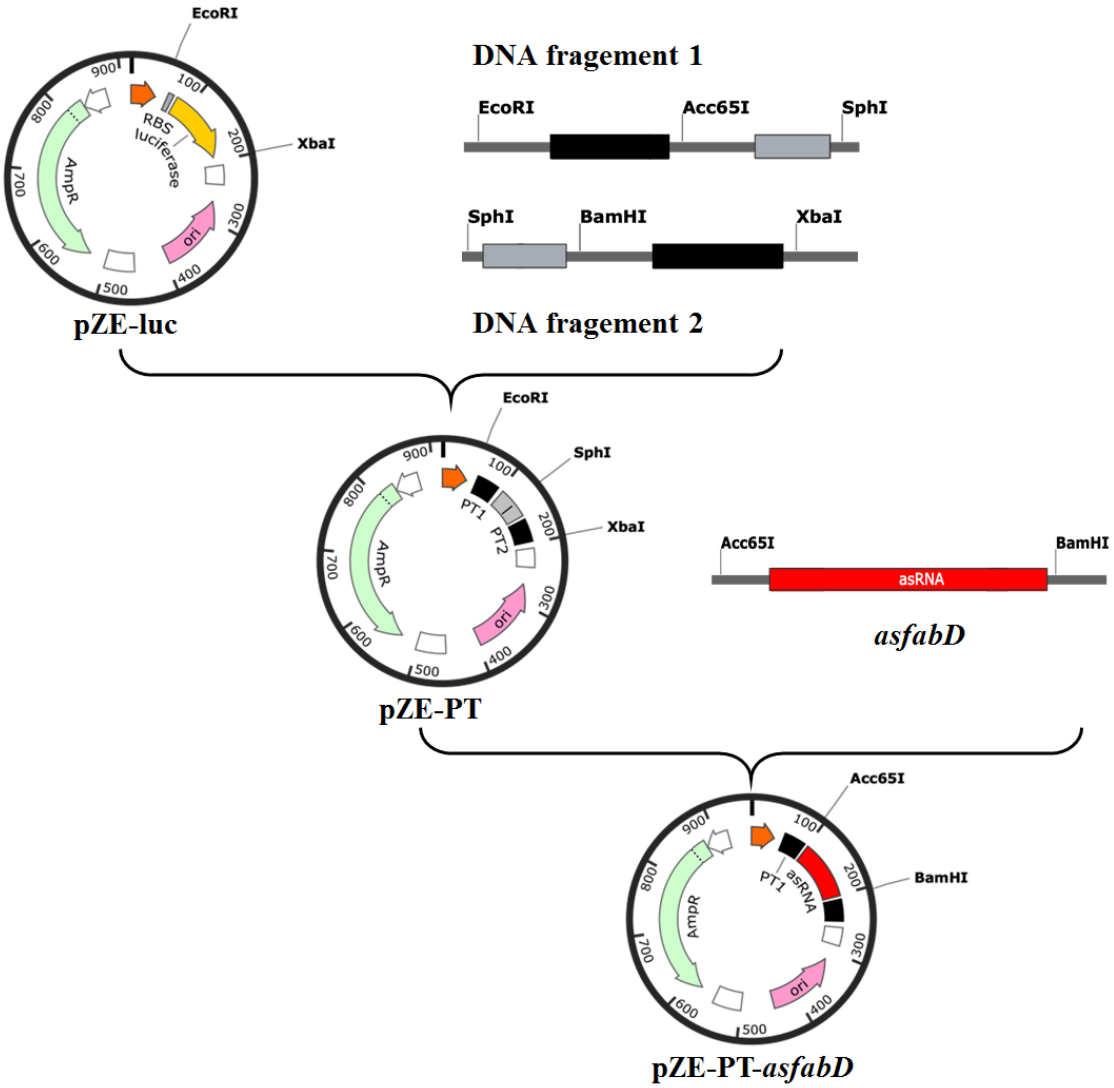


**Figure 3.2** The plasmid construction of pZE-PT-*asfabD*. DNA fragment 1 and DNA fragment 2 were inserted into pZE-luc in between *Eco*RI and *Sph*I, *Sph*I and *Xba*I respectively, to generate parent plasmid pZE-PT. The DNA sequence of *asfabD* was inserted into plasmid pZE-PT in between *Acc65*I and *BamHI* to produce pZE-PT-*asfabD*.

6. Prepare a ligation mixture. DNA fragment 1 and 2: 5 µl (each), plasmid pZE-luc: 2 µl, 2×ligation buffer: 13 µl, ligase: 1 µl, total volume: 26 µl. Wait for 20 min at room temperature and then proceed for transformation.

7. Transfer all the reaction mixture of ligation into 50 μl chemical competent cell *E. coli* XL-Blue. Keep on ice for 20 min. Then heat shock at 42 ℃ for 90 sec. Keep on ice for 2 min. Add 1 ml LB medium into the mixture.

8. Put the culture into the shaker for 40 min at 37 ℃. Centrifuge the culture at 4,000 rpm for 3 min. Discard the supernatant and resuspend the cell pellet in 100 μl LB medium. Spread them on the LB agar plate containing 100 mg/L ampicillin. Incubate the plate overnight at 37 ℃.

9. Pick three transformants and incubate them into 3 ml LB liquid broth at 37 ℃ for 12 hrs.

10. Collect the cell by centrifuge at 12,000 rpm for 1 min. Extract the plasmid by plasmid miniprep kit. Add 50 μl di$H_2O$ to elute the plasmid DNA.

11. Verify the plasmids by *Spe*I and *Sph*I. Prepare mixture of enzyme digestion as following: di$H_2O$: 6 μl, DNA: 2 μl, 10×buffer: 1 μl, enzymes: 0.5 μl (each), total volume: 10 μl (*see* Note 3.5.5).

3.4.1.2 Construct parent plasmid pZE-PT-asfabD (see Note 3.5.6):

1. Amplify the gene *asfabD* by PCR reaction. Dilute primer 5 and 6 using di$H_2O$ to 1 μM. Prepare the PCR mixture (50 μl) using Phusion High-Fidelity DNA polymerase as following: di$H_2O$: 31.5 μl, 10×buffer: 10 μl, 2 mM dNTP: 5 μl, primer 5 and 6: 1 μl (each), genomic DNA: 1 μl, enzyme: 0.5 μl. The PCR product is 100 nt (*see* Note 3.5.7).

2. Purify the DNA product using the same method as 3.4.1.1.3. Add 30 μl di$H_2O$ for elution.

3. Prepare digestion mixture. For DNA fragment as*fabD*: di$H_2O$: 17 μl, DNA: 15 μl, 10×buffer: 4 μl, enzymes: 2 μl (each), total volume: 40 μl. For parent plasmid pZE-PT: di$H_2O$: 26 μl, DNA: 6 μl, 10×buffer: 4 μl, enzymes: 2 μl (each), total volume: 40 μl. Incubate the digested mixture at 37 ℃ for 2-4 hrs in a water bath(*see* Note 3.5.8).

4. Purify the digested product. For DNA fragment as*fabD*: we use the same method as 3.4.1.1.3. But, we add 6 μl di$H_2O$ for elution. For parent plasmid pZE-PT: we used the same method as 3.4.1.1.5, but we add 6 μl di$H_2O$ for elution.

5. Prepare ligation mixture. DNA fragment as*fabD*: 4 μl, plasmid pZE-PT: 1 μl, 2×ligation buffer: 5.5 μl, Quick DNA ligase: 0.5 μl, total volume: 11 μl. Place the reaction tube at room temperature for 20 min.

6. Heat-shock transformation and plasmid verification of pZE-PT-*asfabD*. We used the same method from 3.4.1.1.7 to 3.4.1.1.11.

### 3.4.2 Interference efficiency detection

3.4.2.1 Direct detection method- qRT PCR (*see* Note 3.5.9)

1. Transform the plasmid pZE-PT-*asfabD* into the target strain *E. coli* BW25113. Transform the parent plasmid pZE-PT into the target strain *E. coli* BW25113 as a negative control (*see* Note 3.5.10). Pick three transformants of pZE-PT-*asfabD* and pZE-PT from the overnight plates, respectively. Incubate these transformants in 3.5 ml LB medium containing ampicillin (100 mg/L) at 37 °C and 290 rpm for 5 hrs.
2. Transfer 2 % cultures into baffled flasks containing 15 ml of M9Y media with 1 mM IPTG at 30 °C and 290 rpm.
3. After 12 hrs, take 500 μl cell cultures and centrifuge at 12,000 rpm for 1 min at 4 °C to pellet cells. Discard the supernatant (*see* Note 3.5.11).

Total RNA purification process:

4. Add 100 μl lysozyme solution (*see* materials 3.2.3.1) to the cell pellet and resuspend by vortexing.
5. Add 0.5 μl 10 % SDS solution. Vortex to mix well.

6. Wait for 5 min at room temperature. Add 350 µl lysis bufer with prepared 2-mercaptoethanol (*see* materials 3.2.3.1). Vortex to mix well.
7. Homogenize the cell lysate: transfer the lysate to a 1.5 ml RNase-free microcentrifuge tube and homogenize using an micro tube homogenizer system with sterile micro-pestle for at least 45 seconds. Centrifuge the homogenate at 3,000 rpm for 5 min at room temperature, then transfer the supernatant to clean RNase-free microcentrifuge tube.
8. Add 250 µl 100 % ethanol to each volume of bacterial cell homogenate. Vortex to mix completely to disperse any visible precipitate that may form after adding ethanol.
9. Transfer the sample (including any remaining precipitate) to a spin column with a collection tube. Centrifuge at 12,000 rpm for 15 sec at room temperature. Descard the flow-trough.
10. Prepare DNase I reaction mixture for on-column treatment as following: 10 × DNase I reaction buffer: 8 µl, resuspended DNase I (3U/µl): 10 µl, RNase-free water: 62 µl, final volume: 80 µl. Add the 80 µl DNase mixture directly onto the surface of the spin column. Incubate at room temperature for 15 min.
11. Add 350 µl Wash buffer I to the spin column. Centrifuge at 12, 000 rpm for 15 sec at room temperature. Discard the flow-through.
12. Add 500 µl Wash buffer II with ethanol to the spin column. Centrifuge at 12,000 rpm for 15 sec at room temperature. Discard the flow-through. Repeat this step.
13. Centrifuge the spin column at 12,000 rpm for 1 min. Insert the spin column into a new collection tube. Add 30 µl RNase-free water into the center of the spin column.
14. Incubate at room temperature for 1 min. Centrifuge spin column and collection tube at 12,000 rpm and room temperature for 1 min.

15. Analyzing RNA concentration and quality by Nanodrop (*see* Note 3.5.12).

First Strand cDNA synthesis:

16. Dilute the denatured RNA to 600 ng/µl. Mix RNA sample and primer in a sterile RNase-free microfuge tube as following: Template RNA: 1 µl, $d(T)_{23}VN$ (50 µM):2 µl, RNase-free $H_2O$: 5 µl. Total volume is 8 µl. Denature sample RNA and primer $d(T)_{23}VN$ at 65 ℃ for 5 min. Spin briefly and put on ice imediately.
17. Add the following components: 2 × Protoscript II reaction mix: 10 µl, 10 × Protoscript II enzyme mix: 2 µl. Incubate the 20 µl cDNA synthesis reaction at 42 ℃ for 1 hrs. Inactivate the enzyme at 80 ℃ for 5 min. (*see* Note 3.5.13).

qRT-PCR reaction:

18. Dilute the cDNA to 12 ng/µl. Dilute the primers to 30 µM. In a 1.5 ml reaction tube on ice, prepare the PCR mixture as following: FastStart SYBR Green Master (ROX): 25 µl, primers (30 µM): 0.5 µl(each), di$H_2O$: 22 µl. Total volume is 45 µl. Mix the solutions carefully by pipetting it up and down. Do not vortex.
19. Pipet 24 µl PCR mix into each PCR reaction vessel. Add 1 µl of template DNA. Mix carefully by pipetting up and down. Seal the tubes with clear tube caps. Keep triplicate for each sample. We choose 16S RNA as a normalizer gene from *E. coli*. By using the primer 7 and 8, the product size of 16S RNA is 150 bp. The product size of target gene *fabD* is 274 bp when using primer 9 and 10 (*see* Note 3.5.14). Set the cycling conditions as following: 95 °C for 30 sec; 95 °C for 10 min; followed by 45 cycles of 95 °C for 15 sec; 58 °C for 30 sec; 72 °C for 20 sec (*see* Note 3.5.15).
20. Conduct a melting curve analysis for each reaction using the following condition: 55 °C to 95 °C; 0.5 °C/read; 1 sec hold; 72 °C for 10 min (*see* Note 3.5.16).

21. Calculate the relative gene expression by the $2^{-\Delta\Delta Ct}$ approximation method (*see* Note 3.5.17).

3.4.2.2 Indirect detection method-fluorescence assay (*see* Note 3.5.18)

Construct plasmid pSA-*pfabD/egfp* (*see* Note 3.5.19):

22. Amplify gene *pfabD* and gene *egfp* by PCR reaction. All procedures are the same as 3.4.1.2.1. Use primer 11 and 12 to amplify gene *pfabD*. Use primer 13 and 14 to amplify *egfp*. Purify the PCR product by gel recovery kit. The procedures are the same as 3.4.1.1.5. Add 40 μl di$H_2O$ for elution (*see* Note 3.5.19).
23. Overlap extension PCR for *pfabD/egfp*. Dilute PCR product of *pfabD* and *egfp* by 5 folds, respectively. Prepare the PCR mixture (50 μl) using Phusion High-Fidelity DNA polymerase as following: di$H_2O$: 31.5 μl, 10×buffer: 10 μl, 2 mM dNTP: 5 μl, primer 11&14: 1 μl (each), diluted *pfabD* and *egfp*: 1 μl (each), enzyme: 0.5 μl. Purify the PCR product by gel recovery kit. The procedures are the same as 3.3.3.1.5. Add 30 μl di$H_2O$ for elution from the spin column.
24. Prepare digestion mixture. For DNA fragment *pfabD/egfp*: di$H_2O$: 22 μl, DNA: 10 μl, 10×buffer: 4 μl, enzymes: 2 μl (each) (*see* Note 3.5.20), total volume: 40 μl. For plasmid pSA74: di$H_2O$: 26 μl, DNA: 6 μl, 10×buffer: 4 μl, Enzymes: 2 μl (each), total volume: 40 μl. Incubate the digested mixture at 37 ℃ for 2-4 hrs in a water bath.
25. The following cloning procedures are the same from 3.4.1.1.5 to 3.4.1.1.11.

Fluorescence Assay

26. Co-transform two plasmids pZE-PT-*asfabD* and pSA-*pfabD/egfp* into target strain *E. coli* BW25113. Co-transform the parent plasmid pZE-PT with pSA-*pfabD/egfp* into *E. coli* BW25113 as a negative control (*see* Note 3.5.21).

Inoculate three transformants of each strain into 3.5 ml LB medium with Ampicillin (100 mg/L) and chloramphenicol (34 mg/L), respectively at 37 °C and 290 rpm for 5 hrs.

27. Transfer 2 % cultures into a black 96-well plate with clear bottom containing 200 µl LB medium with 1mM IPTG. eGFP fluorescence is monitored by spectrometer (Biotek) with a time duration of 24 hrs. Set the conditions as following: Temperature: Setpoint 37 °C; Start Kinetic [Run 24:00:00, Interval 0:20:00], Shake: Medium for 16:30, Read: (A) 600, Read: (F) 485/20nm, 528/20nm; End Kinetic. Set the reading type as endpoint mode. (*see* Note 3.5.22).
28. Subtract the background cell fluorescence of each sample and normalize the eGFP fluorescence intensity of each sample against its $OD_{600.}$

**3.5 Notes**

1. To keep a high abundance of asRNAs, we utilized high copy number plasmid pZE-luc for the construction of asRNA plasmid. Parent plasmid pZE-PT consisting of a random DNA sequence in between the two PT sequences, which serves as the basis for constructing various asRNA scaffold plasmids (*see* Figure 3.1(a)).
2. Since the inverted repeat sequences are consisted of GC-rich nucleotides, the whole PT sequence is hard to be amplified by overlap extension PCR. Thus, we divided the whole PT sequence into two part including DNA fragment 1 and DNA fragment 2 (*see* Figure 3.2).
3. Since the size of DNA fragment 1 and 2 is small, we use 30 µl di$H_2O$ to elute DNA product to increase the recovery efficiency.
4. We use enzymes *EcoR*I and *Acc65*I to digest DNA fragment 1 and use enzymes *BamH*I

and *Xba*I to digest DNA fragment 2. For the pZE-luc plasmid, we use enzymes *EcoR*I and *Xba*I for the digestion.

5. When verifing the plasmid, we recommend that the two chosen enzyme restriction sites are located in plasmid and the target DNA, respectively
6. By replacing target-binding sequence, we can generate various new synthetic asRNAs.
7. Primer 5 is reversely complementary to the target gene *fabD* starting from the +30 nt coding region. Primer 6 is identical to the target gene *fabD* starting from -70 nt ahead of the coding region.
8. We use enzymes *Acc65*I and *BamH*I to digest *asfabD* fragment and plasmid pZE-PT.
9. Since asRNA triggered mRNA degradation is the main mechanism of asRNA inhibition, the real-time PCR is the direct method for the identification of interference efficiency at the RNA level.
10. The strain containing plasmid pZE-PT would show higher mRNA concentration of *fabD* than the strain containing plasmid pZE-PT-*asfabD*.
11. For better results, the cells in log-phase growth are optimal to isolate RNA. To prevent RNA degradation, it is important to disrupt the cells fast and completely.
12. Before each experiment, clean your bench and relative equipment by 70 % ethanol. During total RNA isolation process, please always wear a mask and frequently replace gloves to avoid RNA contamination or degradation. The ratio of $OD_{260/280}$ is used to measure RNA purity. An $OD_{260/280}$ >1.8 indicates that RNA is reasonably clean of proteins and other UV chromophores that could negatively affect the stability of the stored RNA.
13. After quantifying the total RNA concentration, we dilute each sample to the same

concentration. Then, we take the same volume of total RNA as the template for the cDNA synthesis in the next step. Heat denaturation of the total RNA is required to open the secondary structure which may impede long cDNA synthesis. .

14. When designing real-time PCR primers for target genes, it is necessary to confirm the primer specificity by the BLAST analysis against the NCBI genome database. To avoid nonspecific bands of the target gene, at least one designed primer should be uniquely homologous to the genomic DNA.
15. It is optional to verify the integrities of the obtained products by gel electrophoresis.
16. Melting curve analysis is necessary and important to assess the specificity of the real-time PCR products. A bi-peak curve indicates a contamination from genomic DNA. A peak in the blank control indicated a contamination from the di$H_2O$ or reagent.
17. We provide an example to describe the detailed calculation process of relative gene expression (*see* Table 3.2) [83]. Use one-tailed unpaired student's T-Test to evaluate the difference between control group and sample group by formula =T. TEST ( Data1 (control), Data 2 (sample), 1, 3). 1 means one-tail t-test. 3 means two sample unequal variance.

**Table 3.2** A detailed calculation process of relative gene expression by $2^{-\Delta\Delta Ct}$ method

| | Reference gene 16S RNA (Ct) | | | Target gene (Ct) | | |
|---|---|---|---|---|---|---|
| C1 | 19.79 | 19.67 | 18.92 | 23.34 | 23.32 | 22.70 |
| C2 | 17.56 | 17.92 | 17.35 | 21.20 | 22.9 | 23.1 |
| C3 | 17.35 | 17.22 | 17.14 | 21.53 | 21.61 | 21.57 |
| S1 | 17.85 | 17.26 | 17.30 | 23.14 | 23.79 | 23.97 |
| S2 | 18.52 | 18.98 | 18.31 | 24.84 | 24.36 | 24.84 |
| S4 | 17.72 | 16.96 | 17.53 | 23.97 | 24.08 | 24.13 |

| | Avg.(R) | Avg.(T) | ΔCt | ΔΔCt | $2^{-\Delta\Delta Ct}$ | Avg. | SD |
|---|---|---|---|---|---|---|---|
| C1 | 19.46 | 23.12 | 3.66 | -0.90 | 1.87 | 1.01 | 0.22 |

| | | | | | | | |
|---|---|---|---|---|---|---|---|
| C2 | 17.61 | 22.40 | 4.79 | 0.23 | 0.85 | | |
| C3 | 17.24 | 21.57 | 4.33 | -0.23 | 1.17 | | |
| S1 | 17.47 | 23.63 | 6.16 | 1.60 | 0.33 | 0.30 | 0.06 |
| S2 | 18.60 | 24.68 | 6.08 | 1.52 | 0.35 | | |
| S4 | 17.40 | 24.06 | 6.66 | 2.10 | 0.23 | | |
| T.TEST | (C2:C3, S1:S3, 1, 3) | | | | | 0.06 | |

18. Fluorescence assay is an alternative detection method of asRNA interference efficiency to save experimental cost. By constructing a *pfabD/egfp* fusion protein with a low copy number plasmid, we detect the expression level of gene *fabD* by monitoring fluorescence signal. However, since the fusion protein is constructed in a plasmid, it is not a direct method to detect asRNA interference efficiency.
19. To maximally simulate the expression of chromosomal genes, we keep the native promoter for gene *fabD* and termed *pfabD*. Remove stop codon of gene *pfabD* and start codon of gene *egfp* when designing the overlap extension PCR primers.
20. We use enzymes *Acc65*I and *BamH*I to digest *pfabD/egfp* fragment and plasmid pSA74.
21. The strain containing parent plasmid pZE-PT and pSA-*pfabD/egfp* would show higher fluorescence intensity than the strain containing asRNA plasmid pZE-PT-*asfabD* and pSA-*pfabD/egfp*.
22. The procedures were applied for real-time monitoring of fluorescence intensity and $OD_{600}$ by Gene5 software in BioTek plate reader.

# CHAPTER 4[1]

ESTABLISHMENT OF AN ARTIFICIAL DYNAMIC REGULATORY NETWORK AND ITS APPLICATION IN METABOLIC ENGINEERING

[1] Yaping Yang, Yuheng Lin, Jian Wang, Yifei Wu, Mengyin Cheng, Ruihua Zhang, Yajun Yan. 2017. To be submitted to Nature.

## 4.1 Abstract

Dynamic pathway regulation is a potential strategy to maximize the metabolic flux through exogenous pathways while maintaining the balanced state of the microbial host's native metabolism. However, the current studies mainly focused on dynamically regulating expression of exogenous pathway genes. Little research report dynamically control of the endogenous competing pathways, especially the essential pathways for cell growth to rewire the metabolic flux towards the target compounds. To address this issue, we designed and established an artificial dynamic regulatory network and demonstrated its effectiveness in improving the biosynthesis of a widely-used platform chemical muconic acid in *Escherichia coli*. Based on a promoter-regulatory system responsive to the generated muconic acid in combination with interference antisense RNA, this system achieved simultaneous up-and-down regulation in an orthogonal manner. With this system, the titer of muconic acid was elevated to the highest level (1.8 g/L) so far observed for this pathway. This artificial regulatory network provided a promising framework to autonomously up-regulate the desirable pathway genes and down-regulate the native competing pathway genes responsive to the changing cellular physiological state for optimal microbial production.

## 4.2 Introduction

Microbial-based metabolic engineering has been extensively utilized for green production of high-value chemicals such as biofuels, biopolymers, nutraceuticals and pharmaceuticals[77]. A fundamental goal of metabolic engineering is to maximize the productivities, yields or titers of desired compounds in microbial hosts. Microorganisms are sophisticated and finely tuned cell factories, and their natural metabolisms are composed of not only enzymatic catalyzed

biochemical reactions but also stringent dynamic regulation on multi-levels epigenetic, transcriptional, translational and allosteric [78]. Via monitoring the states and surpluses within different metabolic networks, microorganisms can balance the catabolism and anabolism, permitting a well-tuned balance of cellular maintenance and metabolites formation[79]. In most cases, however, metabolic engineering induced perturbations to natural metabolism will lead to metabolic imbalances, which include but are not limited to: (1) drain intracellular metabolites due to overexpression of exogenous pathways or systematic deletions of endogenous pathways; (2) cell toxicity ascribed to expression of toxic enzymes, interference of essential metabolite pools or generation of toxic intermediates; (3) cellular resource burdens steming from unbiased or deregulated expression of a large number of heterologous enzymes. The direct outcome of metabolic imbalance is impairment of biomass formation and thereafter compromised product formation.

To address these issues, current advances in metabolic engineering are mostly focused on static optimization of exogenous pathways. These strategies include modulating enzyme expression levels via promoter or ribosome binding site engineering, increasing catalytic turnover of enzymes via protein engineering, colocalizing pathway enzymes via synthetic protein scaffolds or compartmentalization[7,80-84]. Alternatively, more viable dynamic optimizations via signaling native intracellular intermediates by cognate biosensors have been exploited to mimic natural dynamic regulations and achieved control over metabolic pathways. Limited proof-of-concept demonstrations have been conducted in *E. coli* by acetyl phosphate biosensor mediated control of the engineered lycopene biosynthesis[11], fatty acid/acyl-CoA (FA/acyl-CoA) biosensor mediated regulation of biodiesel production[12] and malonyl-CoA sensor mediated regulation of fatty acids biosynthesis[13]. Intermediate-dependent dynamic control permitted alleviation of

metabolic imbalances and real-time alterations of carbon fluxes in response to intermediate fluctuation, which however, are endowed with intrinsic drawbacks including (1) limited dynamic sensitivity or range[10], (2) production lagging elicited by inevitable oscillation of intracellular intermediates[13] and (3) undermined robustness and sustainability in production. Yet the simple dynamic coupling of exogenous pathways to intermediate levels were mostly monofunctional and suboptimal because of the biased biomass formation over production.

In the present study, we sought to reconstitute and functionalize a ubiquitous dynamic system based on end-product biosensors that broadly exist in different microbial contexts, and investigated its potency and applicability in metabolic engineering. The multi-task modulation nature of this system enables switching on biosynthetic routes of desired products and switching off competing pathways in a reciprocal and escalating fashion, so as to achieve an autonomous and optimal tradeoff between growth-sustainment and product-formation. The developed control elements consist of sensor-regulator and RNA interference technique. The sensor-regulator triggers gene expression by sensing cellular metabolites, which provides the up-regulation function. When this function is used to initiate antisense RNA (asRNA) synthesis for repressing different target gene expression, the opposite function, orthogonal down-regulation, can be realized simultaneously (Figure 4.1). To validate the design of such an end product-oriented dynamic system, we

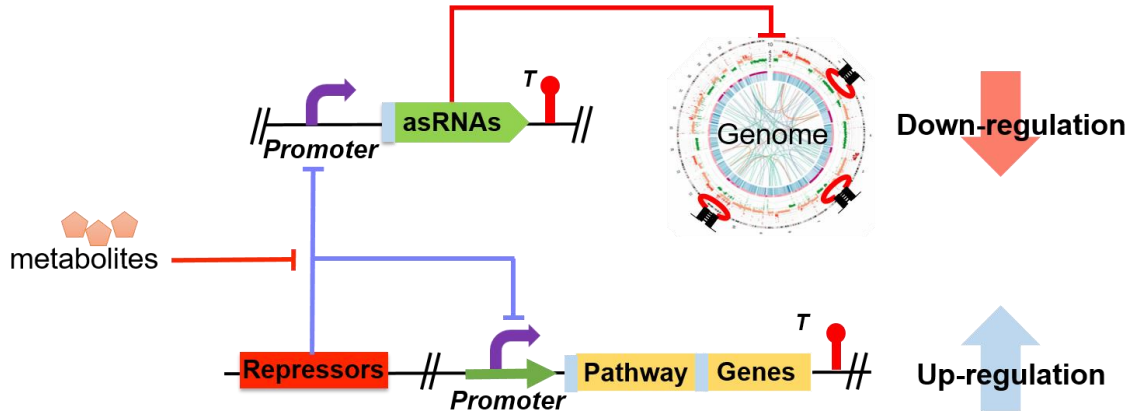


**Figure 4.1** The scheme of artificial dynamic regulatory network

constructed and characterized on a noncognate muconic acid (MA)-mediated promoter-regulatory system in *E. coli* and developed a prototype of the dynamic regulatory network to control the expression of different fluorescence proteins for testing (Figure 4.2). The expected logic control should be like this: first, the end product MA served as the inducer in the system; second, at the beginning, the system was focused on the cell growth; third, when the cell growth was not the dominate factor, the secondary metabolite formed and MA accumulated; finally, the accumulated MA would serve as signal to up-regulate the upstream EP module genes and down-regulate the competing pathway genes to redirect the carbon source from the TCA cycle to the MA biosynthesis pathway. Based on a promoter-regulator system responsive to generated MA, this system was combined with interference antisense RNA (asRNA) to achieve simultaneous up and down regulation.

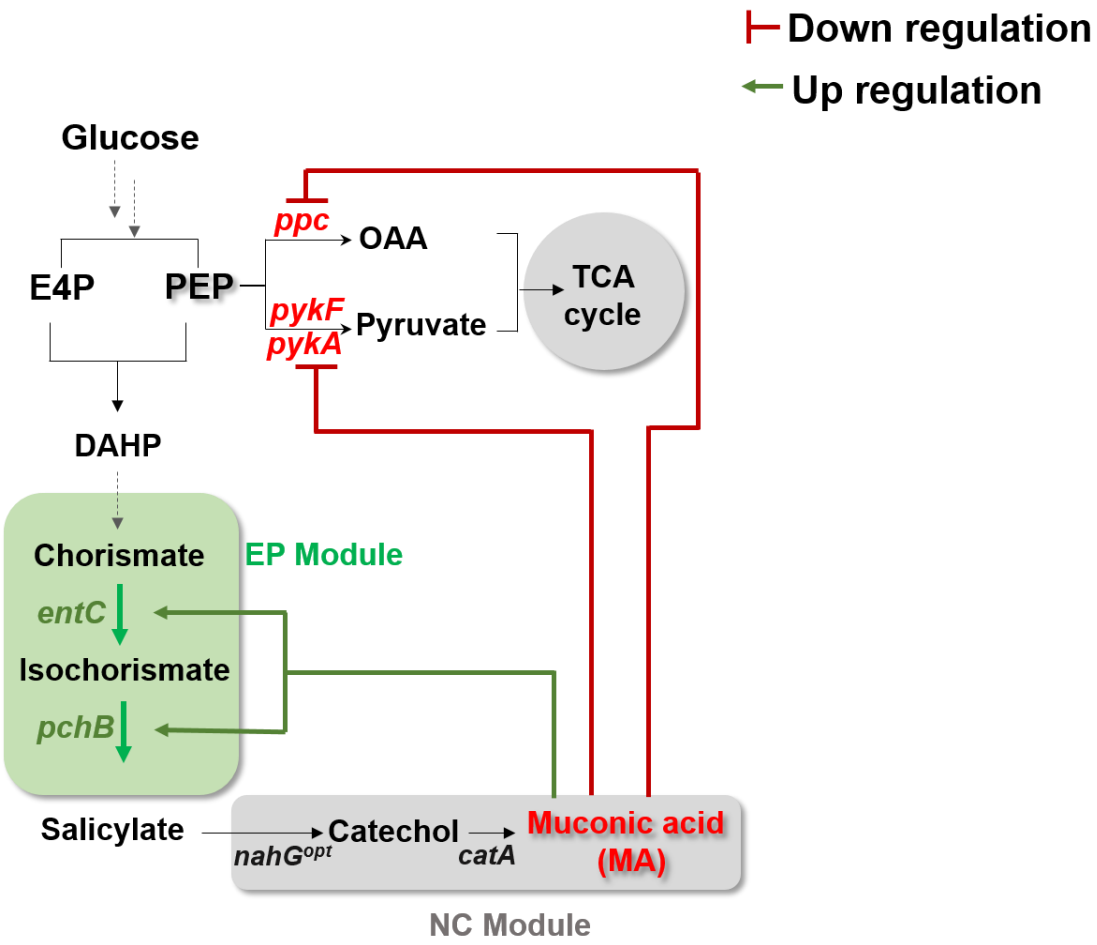


**Figure 4.2** The scheme of applying the dynamic regulatory network to the MA biosynthesis pathway.

## 4.3 Methods and Materials

### 4.3.1 Experimental materials

Luria-Bertani (LB) medium was used for *E. coli* inoculation and plasmid propagation. The minimum medium M9Y contains (per liter): glycerol (15 g), yeast extract (5 g), $NH_4Cl$ (1 g), $Na_2HPO_4$ (6 g), $KH_2PO_4$ (3 g), NaCl (0.5 g), $MgSO_4 \cdot 7H_2O$ (2 mmol), $CaCl_2 \cdot 2H_2O$ (0.1 mmol) and vitamin B1 (1.0 mg). 100 mg/L of ampicillin, 50 mg/L of kanamycin and/or 34 mg/L of chloramphenicol were added to the medium when necessary. The *E. coli* strain XL1-Blue was

used as the host strain for plasmid construction, and strain BW25113/F' was used for the biosynthesis of muconic acid. Plasmids pZE12-luc, pCS27 and pSA74 are respectively the high, medium and low copy number plasmids employed for pathway assembly in this work (see **Table 3.1** for a list of all strains and plasmids used in this study).

$P_{MA}$ promoter and *catR* gene (GenBank accession number SKC04124.1) were from *P. putida* KT2440 purchased from ATCC (ATCC number: 47054D-5). RFP gene (GenBank accession number AMO27245.1) was a kind gift from Dr. Gang Cheng group at the Chemical and Biomolecular Engineering Department of University of Akron (OH, USA).

Phusion High-Fidelity DNA polymerase, DNase I, restriction endonucleases and Quick Ligation Kit were purchased from New England Biolabs (Beverly, MA, USA). Zyppy™ Plasmid Miniprep Kit, Zymoclean™ Gel DNA Recovery Kit, and DNA Clean & Concentrator™-5 were purchased from Zymo Research (Irvine, CA, USA). Muconic acid standard was purchased from ACROS ORGANICS (Bridgewater, NJ, USA).

### 4.3.2 Strain construction

To create the *E. coli* strain YYP1 that was chromosomally integrated with an eGFP gene, the $P_{LlacO-1}$-eGFP cassette was amplified from pZE-p$P_{LlacO-1}$-eGFP and inserted into the *E. coli* BW25113/F' genome between the *nupG* and *speC* loci via Red recombination method[85, 86] (see **Table 4.1** for a list of all strains used in this study). *E. coli* BW25113/F' knockout derivatives YYP2 (Δ*pykF*Δ*pykA*) and YYP3 (Δ*pykF*Δ*pykA*Δ*ppc*) were created via P1 phage transduction method ( https://openwetware.org/wiki/Sauer:P1vir_phage_transduction).

**Table 4.1** Strains and plasmids used in Chapter 4

| **Strain** | **Genotype** | **Source** |
|---|---|---|
| *E. coli* XL1-Blue | *recA1 endA1 gyrA96 thi-1 hsdR17 supE44 relA1 lac*[*F'proAB lacI*$^{q}$*ZΔM15 Tn10 (Tet*$^{r}$*)*] | Stratagene |
| *E. coli* BW25113/F' | *rrnBT14* Δ*lacZWJ16 hsdR514* Δ*araBADAH33* Δ*rhaBADLD78* | This study |
| YYP1 | *E. coli* BW25113/F' integrated with $P_{LlacO-1}$-eGFP cassette between *nupG* and *speC* loci | This study |
| YYP2 | *E. coli* BW25113/F' with *pykF* and *pykA* disrupted | This study |
| YYP3 | YYP2 with *ppc* disrupted | This study |
| **Plasmid** | **Description** | **Source** |
| pZE12-luc | $P_{LlacO-1}$, colE ori, luc, Amp$^{r}$ | Lin[87] |
| pCS27 | $P_{LlacO-1}$, P15A ori, Kan$^{r}$ | Lin[87] |
| pSA74 | $P_{LlacO-1}$, pSC101 ori, Cm$^{r}$ | Lin[87] |
| pZE-p$P_{LlacO-1}$-PT | pZE12-luc harboring PT sequence under the control of $P_{LlacO-1}$ promoter | Yang[16] |
| pZE-p$P_{MA}$-PT | pZE12-luc harboring PT sequence under the control of $P_{MA}$ promoter | This study |
| pZE-p$P_{LlacO-1}$-eGFP | pZE12-luc harboring $P_{LlacO-1}$-eGFP | Yang[16] |
| pZE-p$P_{MA}$-eGFP | pZE12-luc harboring $P_{MA}$-eGFP | This study |
| pSA-p$P_{lpp}$-CatR | pSA74 harboring CatR under the control of $P_{lpp}$ promoter | This study |
| pZE-p$P_{MA}$-eGFP-p$P_{lpp}$-CatR | pZE12-luc harboring $P_{MA}$-eGFP and $P_{lpp}$-CatR | This study |
| pZE-p$P_{MA}$-as*egfp*(100) | pZE-p$P_{MA}$-PT harboring 100 bp as*egfp* DNA under the control of $P_{MA}$ promoter | This study |
| pCS-p$P_{MA}$-RFP | pCS27 harboring $P_{MA}$-RFP | This study |
| pZE-p$P_{LlacO-1}$-EP | pZE12-luc harboring *entC* and *pchB* under the | Lin[87] |

| | | |
|---|---|---|
| pSA-pP$_{LlacO-1}$-NC | pSA74 harboring *nahG*$^{opt}$ and *catA* under the control of P$_{LlacO1}$ promoter<br>pSA74 harboring *nahG*$^{opt}$ and *catA* under the control of P$_{LlacO-1}$ promoter | Lin[87] |
| pZE-pP$_{MA}$-EP | pZE12-luc harboring P$_{MA}$-EP | This study |
| pSA-pP$_{LlacO-1}$-NC-pP$_{lpp}$-CatR | pSA74 harboring P$_{LlacO-1}$-NC and P$_{lpp}$-CatR | This study |
| pZE-pP$_{LlacO-1}$-EP-pP$_{MA}$-as*pykF*(100)-pP$_{MA}$-as*pykA*(100) | pZE12-luc harboring P$_{LlacO-1}$-EP, P$_{MA}$-as*pykF*(100) and P$_{MA}$-as*pykA*(100) | This study |
| pZE-pP$_{LlacO-1}$-EP-pP$_{LlacO1}$-aspykF(100)-pP$_{LlacO-1}$-as*pykA*(100) | pZE12-luc harboring P$_{LlacO-1}$-EP, P$_{LlacO1}$-as*pykF*(100) and P$_{LlacO-1}$-as*pykA*(100) | This study |
| pZE-pP$_{MA}$-EP-pP$_{MA}$-as*pykF*(100)-pP$_{MA}$-as*pykA*(100) | pZE12-luc harboring P$_{MA}$-EP, P$_{MA}$-as*pykF*(100) and P$_{MA}$-as*pykA*(100) | This study |

### 4.3.2 DNA manipulation

For initial characterization of the P$_{MA}$ promoter regulatory system, the P$_{MA}$ promoter sequence was amplified from genomic DNA of *P. putida* KT2440 and used to replace the P$_{LlacO-1}$ promoter of pZE-pP$_{LlacO-1}$-eGFP using *Xho*I and *Eco*RI to generate pZE-pP$_{MA}$-eGFP. Likewise, the *catR* gene was amplified from *P. putida* KT2440 and used to replace the eGFP of pSA-pP$_{lpp}$-eGFP using *Bsr*GI and *Bam*HI to generate pSA-pP$_{lpp}$-CatR. The P$_{lpp}$-CatR operon was amplified and cloned into pZE-pP$_{MA}$-eGFP between *Spe*I and *Sac*I, yielding pZE-pP$_{MA}$-eGFP-pP$_{lpp}$-CatR. Similarly, a parent plasmid pZE-pP$_{MA}$-PT was generated from pZE-pP$_{LlacO-1}$-PT by replacing the P$_{LlacO-1}$ promoter with P$_{MA}$ promoter using *Xho*I and *Eco*RI. The 100 bp DNA sequence of *egfp* asRNA was cloned into pZE-pP$_{MA}$-PT using *Acc*651 and *Bam*HI, resulting pZE-pP$_{MA}$-*asegfp*(100) as asRNA synthesis plasmid. The *rfp* gene was used to replace eGFP of pZE-pP$_{MA}$-

eGFP using *Acc*651 and *Xba*I to generate pZE-p$P_{MA}$-RFP. The $P_{MA}$-RFP operon was subcloned and inserted into pCS27 using *Spe*I and *Sac*I, yielding pCS-p$P_{MA}$-RFP.

To generate pZE-p$P_{MA}$-EP, the *entC-pchB* operon was amplified from previously constructed plasmid pZE-p$P_{LlacO-1}$-EP[6] and was used to replace eGFP of pZE-p$P_{MA}$-eGFP between *Acc*651 and *Xba*I. The $P_{lpp}$-CatR operon was cloned into a previously constructed plasmid pSA-p$P_{LlacO-1}$-NC using *Spe*I and *Sac*I, yielding pSA-p$P_{LlacO-1}$-NC-p$P_{lpp}$-CatR. The 100 bp DNA sequences of *pykF* and *pykA* asRNAs were cloned into pZE-p$P_{MA}$-PT using *Acc*651 and *Bam*HI, resulting pZE-p$P_{MA}$-*aspykF*(100) and pZE-p$P_{MA}$-*aspykA*(100), respectively. The $P_{MA}$-*aspykF*(100) and $P_{MA}$-*aspykA*(100) operons were cloned into plasmid pZE-p$P_{LlacO-1}$-EP using *Spe*I, *Nhe*I, and *Sac*I, yielding plasmid pZE-p$P_{LlacO-1}$-EP-p$P_{MA}$-*aspykF*(100)-p$P_{MA}$-*aspykA*(100). Similarly, the plasmid pZE-p$P_{LlacO-1}$-*asppc*(100) and pZE-p$P_{MA}$-*asppc*(100) were generated. The $P_{LlacO-1}$-*asppc*(100) and $P_{MA}$-*asppc*(100) operons were cloned into pZE-p$P_{LlacO-1}$-EP or pZE-p$P_{MA}$-EP using *Spe*I and *Sac*I, yielding pZE-p$P_{LlacO-1}$-EP-p$P_{LlacO-1}$-*asppc*(100), pZE-p$P_{LlacO-1}$-EP-p$P_{MA}$-*asppc*(100), and pZE-p$P_{MA}$-EP-p$P_{MA}$-*asppc*(100).

### 4.3.4 Culturing conditions

For muconic acid bioproduction, all transformants of BW25113/F' or its knockout mutants were cultured in 3.5 ml LB medium with appropriate antibiotics at 37 ℃ and 290 rpm for 7 hrs. Then 2% cultures were transferred into 125-ml baffled flasks containing 20 ml of M9Y media and cultivated at 30 ℃ shaker and 290 rpm for 48 hrs. When needed, isopropyl β-D-1-thiogalactopyranoside (IPTG) was added to the medium during culture transfer with a final concentration of 0.5 mM. 1 ml culture was sampled to measure cell optical density at 600 nm ($OD_{600}$) and analyze the products by HPLC every 8 hrs.

### 4.3.5 HPLC-quantitative analysis

Both the standards and samples were analyzed and quantified by reverse phase HPLC (Dionex Ultimate 3000) equipped with a ZORBAX SB-C18 column and an Ultimate 3000 photodiode array detector. Solvent A was water with 0.1% formic acid, and solvent B was methanol. The column temperature was set to 28 ℃. The HPLC program was set at a flow rate of 1 ml/min with gradient concentration: 5-50% solvent B for 15 min, 50-5% solvent B for 1 min, and 5% solvent B for an additional 4 min. Quantification of muconic acid was based on the peak areas at absorbance of 260 nm.

### 4.3.6 Fluorescence assay

For fluorescence assay *E. coli* BW25113/F' transformants containing eGFP or RFP expression plasmids were cultured in 3.5 ml LB medium with appropriate antibiotics at 37 ℃ and 290 rpm for 7 hrs. Then 2% cultures (4 μl) were transferred into a black 96-well plate with clear bottom (BRAND plates) containing 200 μl of LB media with various concentrations of muconic acid (0 mM, 0.2 mM, 1 mM, 5 mM) and appropriate antibiotics. The plate was incubated in the Synergy HT (BioTek) plate reader with medium continuous shaking at 37 °C for 24 hrs. Cell optical density was measured at $OD_{600}$ and fluorescence intensity was recorded using the following parameters.The eGFP fluorescence intensity was detected by an excitation filter of 485/20 nm with an emission filter of 528/20 nm. The RFP fluorescence intensity was detected by excitation filter of 530/25 nm with an emission filter of 590/35 nm. The measurement interval was set to be 20 min for each sample. The eGFP or RFP fluorescence intensity of each sample was obtained from three independent measurements and subtracted with the background cell fluorescence of

the control group. The reading type was set as endpoint mode. The activation efficiency (a.e., effect of down-regulation) was calculated as following:

$$\text{a. e.} = \frac{\text{Intensity}_{\text{induced}} - \text{Intensity}_{\text{bacground}}}{\text{Intensity}_{\text{uninduced}} - \text{Intensity}_{\text{bacground}}}.$$

The interference efficiency (i,e., effect of down-regulation) was calculated as following:

$$\text{i. e.} = \frac{\text{Intensity}_{\text{uninduced}} - \text{Intensity}_{\text{induced}}}{\text{Intensity}_{\text{uninduced}} - \text{Intensity}_{\text{bacground}}}.$$

## 4.4 Results

### 4.4.1 Characterization of an MA promoter-regulator system

To construct a muconic acid promoter-regulatory system, we tested a natural muconic acid-responsive transcription factor, CatR, from the *Pseudomonas putida*. CatR is a member of the LysR family, which is a DNA-binding protein involved in regulation of the phenol and benzoate degradation gene cluster (*catBCA*) in response to MA[88-90]. The protein-protein interaction between CatR dimers forms a tetramer which binds to a 26-bp DNA sequence (termed as repression binding sequence, rBS) and a 14-bp adjacent region (termed as activation binding sequence, aBS) in the catBCA promoter (named $P_{MA}$ promoter here) in the absence of MA. Since the aBS sequence overlaps with the -35 region of catBCA promoter, the binding of CatR tetramer to the rBS and aBS sequence triggers a DNA bending and blocks the RNA polymerase from initiating expression of catBCA[89]. The binding of MA to CatR tetramer triggers a conformational change, resulting in relaxing the DNA bending and recruiting the RNA polymerase to activate the expression of downstream genes (Figure 4.3)[91].

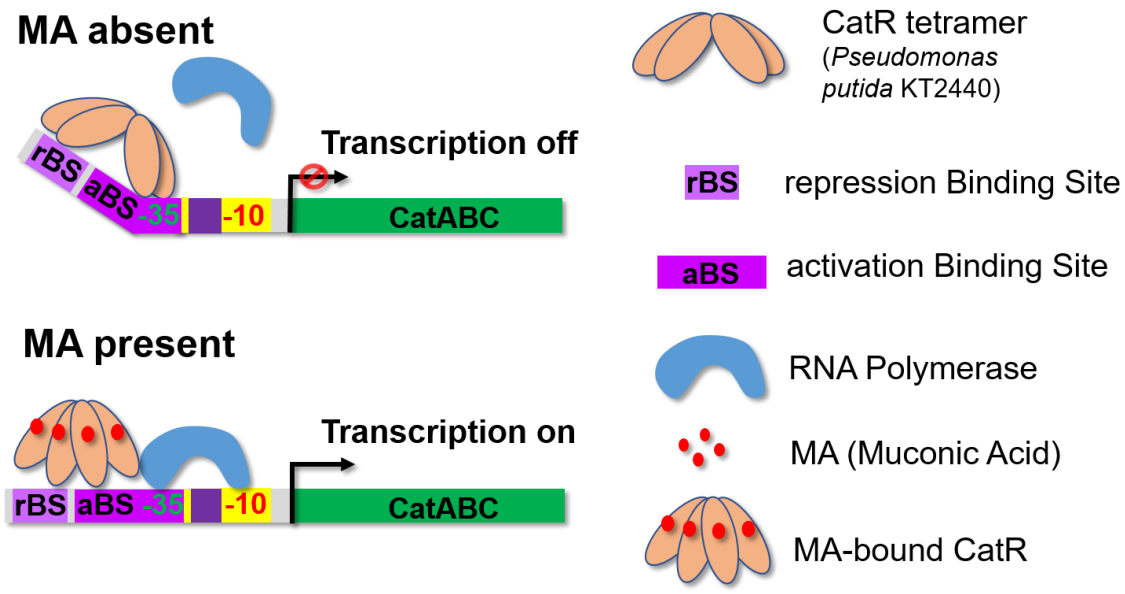


**Figure 4.3** The schematic of promoter-regulatory system responsive to MA.

To express *catR* in *E. coli*, gene *catR* was inserted into the high-copy number plasmid pZE12-luc under control of a constitutive promoter $P_{lpp}$, resulting in pZE-p$P_{lpp}$-CatR. Then, we created a reporter system by inserting the 40-bp CatR binding sequence (rBS and aBS) ahead of *egfp* gene encoding an enhanced green fluorescence protein, resulting in pZE-p$P_{MA}$-*egfp*-p$P_{lpp}$-CatR (Figure 4.4a). In the absence of MA, CatR is expected to block the RNA polymerase by binding to the $P_{MA}$ promoter, turning off *egfp* transcription. When MA is present, formation of CatR-rBS-aBS complex is expected to recruit RNA polymerase, initiating *egfp* transcription (Figure 4.4a).

We firstly evaluated the dynamic range of CatR-$P_{MA}$ promoter regulatory system. When exogenously fed with MA, *E. coli* BW25113/F' containing pZE-p$P_{MA}$-*egfp*-p$P_{lpp}$-CatR showed MA-dependent activation of fluorescence over a broad concentration range from 0.2 mM to 5 mM, whereas no induction of $P_{MA}$ promoter activity was observed in the absence of MA (Figure 4.4b). Especially, a 22-fold fluorescence change was observed upon addition of 5 mM MA, even

greater than the 17-fold fluorescence change of the *egfp* expression under the control of $P_{LlacO-1}$ promoter on the high copy number plasmid pZE-p$P_{LlacO-1}$-eGFP when induced by 0.5 mM IPTG (Figure 4.4b). This indicated that $P_{MA}$ promoter was sensitive and robust to MA induction.

To validate if the changed promoter recognition element or promoter spacer may expand the dynamic range[92], we designed and constructed several mutated or hybrid promoters by changing the sequence between -35 and -10 regions of the wild type $P_{MA}$ promoter. We mutated A at the -12 position of the wild type $P_{MA}$ promoter into T based on the report that this mutation was able to greatly improve the promoter strength[92], resulting in promoter $P_{mut(12AT)}$. By replacing the -35 and -10 regions of the wild type $P_{MA}$ promoter with those of $P_{LlacO-1}$, which is a strong promoter used in *E. coli* [48], we generated a hybrid promoter named $P_{hyb(-35,-10)}$. In addition, another hybrid $P_{hyb(Llac)}$ promoter was created by completely replacing the promoter sequence region of the wild type $P_{MA}$ promoter with the sequence spanning from the transcription start point to the -35 region in $P_{LlacO-1}$ promoter. However, based on the result of eGFP fluorescence assay, these mutated or hybrid promoter-regulators showed similar dynamic range even lower sensitivity than the wild type $P_{MA}$ promoter (see supporting information, Figure 5.1b to 5.1e). Thus, we chose the wild type $P_{MA}$ promoter for the following study.

To test the contribution of CatR abundance on the $P_{MA}$ promoter induction[93], we amplified and inserted p$P_{lpp}$-CatR into a low-copy number plasmid pSA74 (pSA-p$P_{lpp}$-CatR) (see supporting information Figure 5.2). Based on the result of eGFP fluorescence assay, the $P_{MA}$ promoter exhibited similar up-regulation activity when CatR was either on high- or low-copy number plasmid, indicating that low expression of CatR was enough for the stringent control of $P_{MA}$ promoter and providing desired dynamic response.

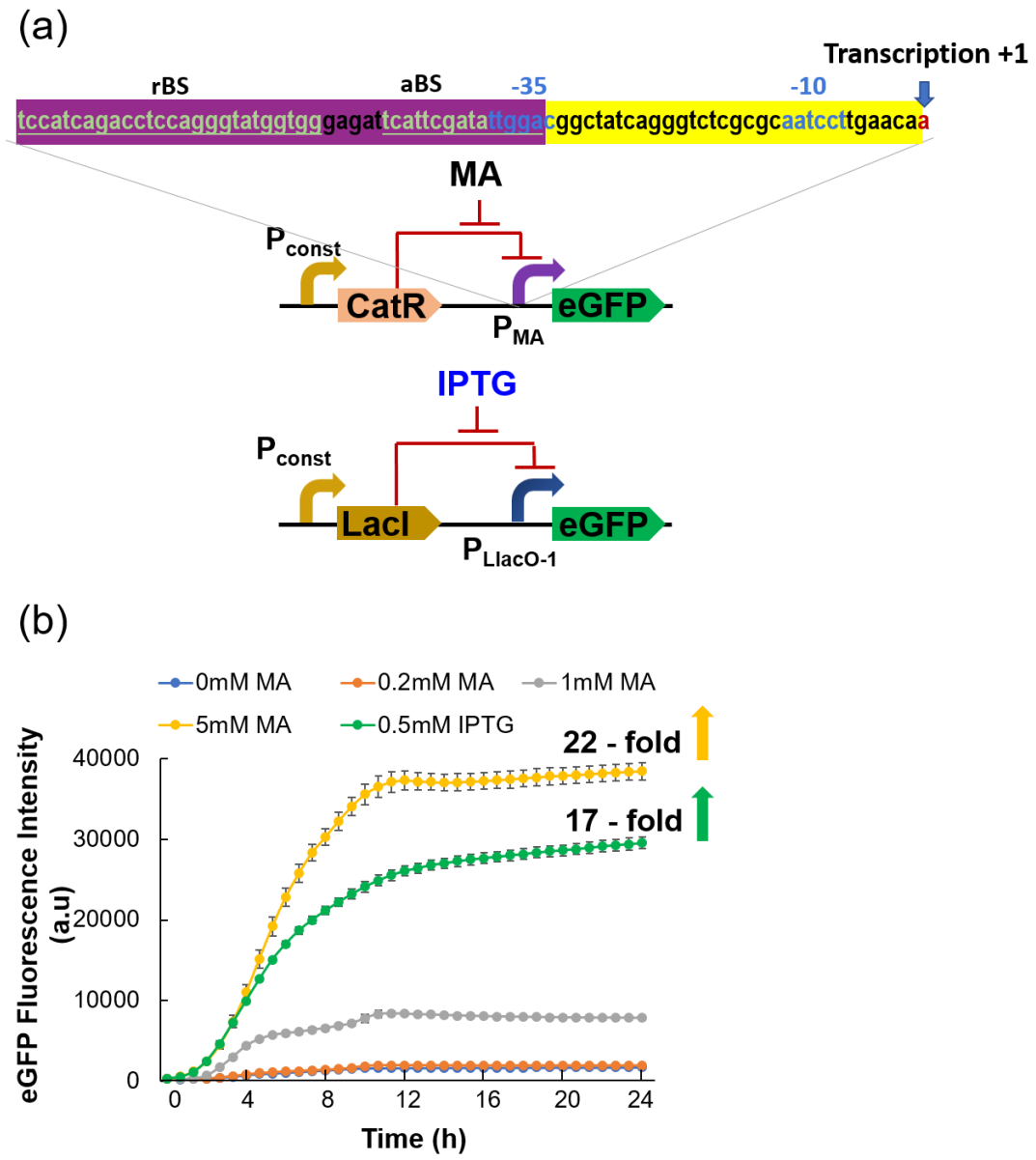


**Figure 4.4** Characterization of a MA-mediated promoter-regulatory system to dynamically modulate the expression of eGFP. (a) The schematic of MA responsive reporter system with $P_{MA}$ promoter sequence. (b) The effect of up-regulation of MA biosensor in response to exogenous muconic acid. 1% of overnight culture of *E. coli* harboring plasmid (pZE-p$P_{MA}$-eGFP-p$P_{lpp}$-CatR or pZE-p$P_{LlacO-1}$-eGFP-p$P_{lpp}$ (negative control)) was transferred into 200uL LB medium. Various amounts of MA or 0.5 mM IPTG (NC) were added to culture as indicated. Fluorescence was

measured at each 40 min during 24 hrs. Data represented the average of three biological replicates, and error bars represented s.d.

### 4.4.2 Dynamic down-regulation by integrating RNAi with the MA promoter-regulator

RNAi is an effective technique to repress gene expression. Through exogenously introducing the asRNAs into the host system, the asRNAs are able to regulate the expression of the target chromosomal and plasmid-carried genes by RNA-RNA interaction in the post-transcriptional level [42]. Without any DNA sequence modification of the target genes, the RNAi can be flexibly implemented to control multiple targets simultaneously, especially those are essential to cell viability[16, 67]. Thus, we integrated RNAi with the MA promoter-regulator to achieve dynamic down-regulation. We have developed asRNAs to conditionally down-regulate the fatty acid biosynthesis to enhance fatty acid derived compounds in our previous study[16]. The constructed asRNAs had a stem-loop structure, in which a pair of 38-nt inverted repeat sequences form the stem to stabilize the design and an RNA fragment forms the loop to target a specific region of mRNA. We had demonstrated that the asRNAs with 100-nt loops binding to the mRNA translation initiation regions covering RBS and start codon provided the superior down-regulation effects[16]. Thus, we kept this design in this study.

To enable down-regulation of any gene in response to MA, we placed asRNA of target genes under control of CatR-$P_{MA}$ system. First, we created a reporter strain *E. coli* YYP1 in which $P_{LlacO-1}$-eGFP cassette was chromosomally integrated between *nupG* and *speC* loci. Next, we designed a 100 nt anti-*egfp* asRNA (as*egfp*) targeting the RBS and coding region of *egfp* and inserted it into pZE12-luc under the control of $P_{MA}$ promoter (pZE-p$P_{MA}$-as*egfp*(100)). When *E. coli* YYP1 was co-transformed with pZE-p$P_{MA}$-as*egfp*(100) and pSA-p$P_{lpp}$-CatR, the eGFP

fluorescence intensity decreased by 0%, 6.2%, 40.6%, and 67.0% when titrating with different concentration of MA (0 mM, 0.2 mM, 1.0 mM, and 5.0 mM) (Figure 4.5). The result indicated that MA induced up-regulation can be transduced into down-regulation through asRNA interference in a dose-dependent manner.

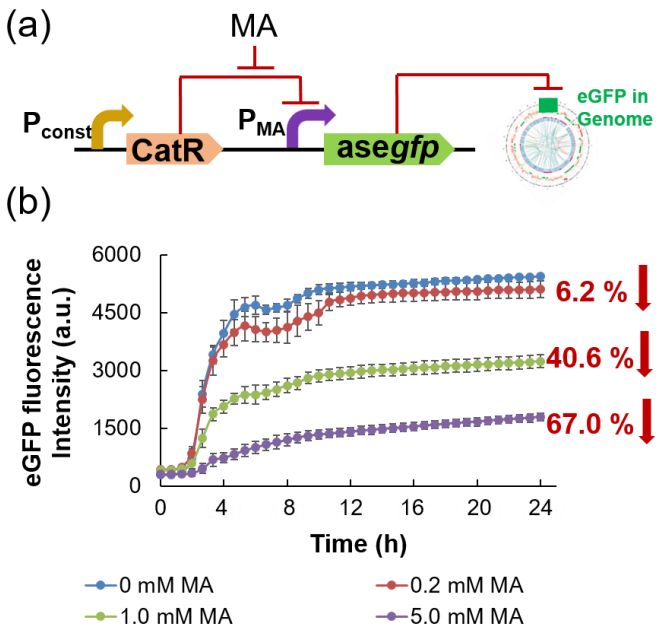


**Figure 4.5** Dynamic down-regulation by integrating RNAi with the MA promoter-regulator. (a) The schematic of MA responsive sensor-regulator and RNAi based dynamic down-regulation. (b)The effect of down-regulation of MA biosensor in response to exogenous MA.

### 4.4.3 Prototyping sensor-regulator and RNAi based dynamic control network

Next, to mimic the naturally existing dynamic regulation system, we attempted to implement CatR-$P_{MA}$ system for simultaneous up- and down-regulation in an orthogonal manner. As the construct of this prototype, the regulator protein CatR was constitutively expressed by plasmid pSA-p$P_{lpp}$-CatR, the reporter *rfp* gene was placed under control of $P_{MA}$ promoter in plasmid pCS-p$P_{MA}$-RFP as the reporter of the up-regulation function; while the antisense *asegfp* was also

placed under the control of $P_{MA}$ promoter in plasmid pZE-p$P_{MA}$-as*egfp*(100) to target the chromosomal *egfp* gene in the *E. coli* strain YYP1, which was used as the reporter of the down-regulation function. When titrating with different concentration of MA (0 mM, 0.2 mM, 1.0 mM, and 5.0 mM), the built prototype system exhibited simultaneous and orthogonal up-regulation and down-regulation in a dose-dependent manner. Particularly, compared with the control strain without MA as inducer, 2.0-, 8.6-, 11.1-fold up-regulation (Figure 4.6a) and 0.27-, 0.48-, 0.60-

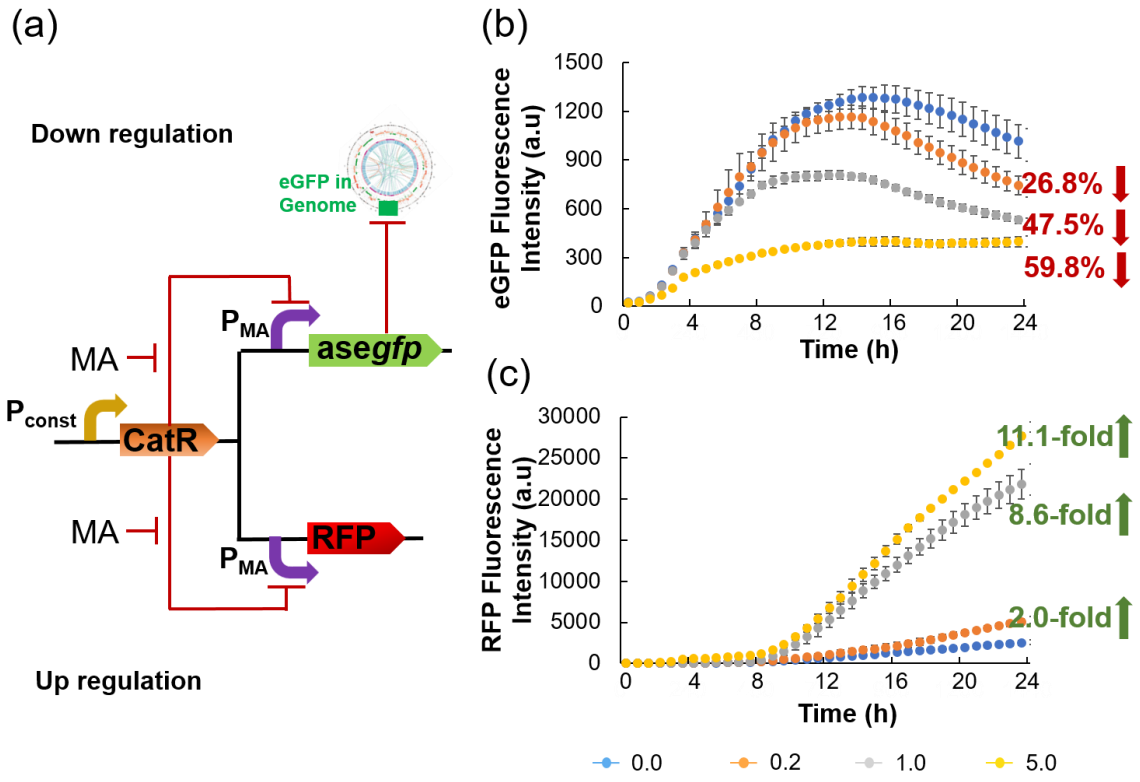


**Figure 4.6** Prototyping sensor-regulator and RNAi based dynamic control network. (a) The schematic of bifunctional up-regulation and down-regulation. (b-c) The effect of simultaneous up- and down-regulation of MA biosensor in response to exogenous MA.

fold down-regulation (Figure 4.6b) were achieved at 24 hours with 0.2 mM, 1.0 mM, 5.0 mM of MA. In general, the constructed dynamic control network in this prototype system was able to achieve similar sensitivity and dynamic responses for both up-regulation and down-regulation functions by sensing the same inducing compound. Overall, the results confirmed the bi-function of the designed dynamic control network at translational level.

### 4.4.4 Applying dynamic control network to MA biosynthesis - up regulation in wild type strain

After validating the regulation capability of CatR-$P_{MA}$ promoter system, we first sought to anchor it to control the metabolic pathway of MA in *E. coli*. We previously developed a MA biosynthetic pathway initiated from the shikimate pathway intermediate chorismate that contained two modules. The upstream EP module is responsible for salicylate (SA) biosynthesis catalyzed by isochorismate synthase (EntC) and isochorismate pyruvate lyase (PfPchB), and the downstream NC module is responsible for bioconversion of SA to MA catalyzed by salicylate 1-monoxygenase ($NahG^{opt}$) and catechol 1,2-dioxygenase (CatA)[5] (Figure 4.2). Modular optimization has demonstrated that high level expression of EP module on pZE12-luc (pZE-EP) and low expression of NC module on pSA74 (pSA-NC) maximized MA production, suggested the relatively high activity of NC module. To render MA biosensor mediated auto-induction, we created two plasmids with the EP module under control of $P_{MA}$ promoter on pZE12-luc and the NC module under the control of $P_{LlacO-1}$ promoter on pSA-$pP_{lpp}$-CatR, namely pZE-$pP_{MA}$-EP and pSA-$pP_{LlacO-1}$-NC-$pP_{lpp}$-CatR. When co-transferred into wild type *E. coli* BW25113/F', the resultant strain produced MA with a maximum titer of 290 mg/L at 48 h without IPTG induction. In contrast, the control strain BW25113/F' harboring pZE-$pP_{LlacO-1}$-EP and pSA-$pP_{LlacO-1}$-NC-

$pP_{lpp}$-CatR only produced 49 mg/L MA without IPTG induction. These results indicated that MA biosensor mediated up-regulation on EP module led to a 5.87-fold increase of MA titer than leaky expression of EP module in the same genetic background and environmental conditions (Figure 4.7).

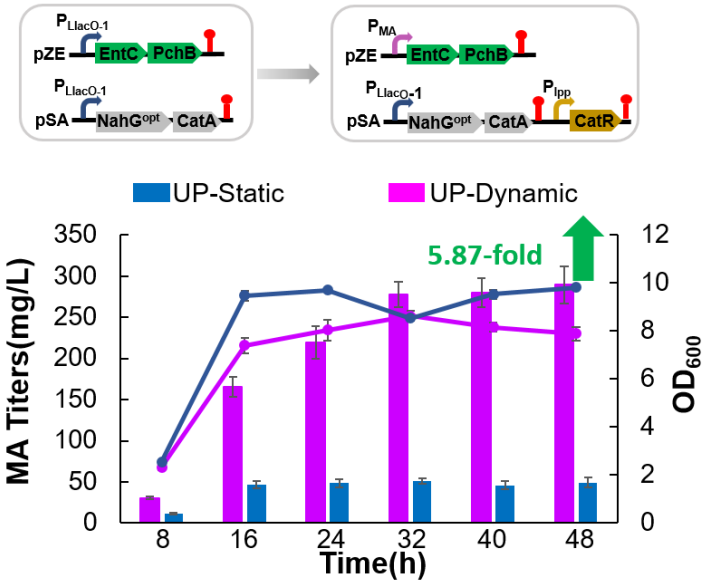


**Figure 4.7** MA production behavior by dynamic MA biosensor mediated up-regulation in wild type strain *E. coli* BW25113/F'. The productivity (cell density and MA titers) of *E. coli* strain BW25113/F' containing $P_{MA}$ promoter mediated EP module ($pP_{MA}$-EP) and control strain *E. coli* BW25113/F' containing $P_{LlacO-1}$ promoter mediated EP module ($pP_{LlacO-1}$-EP) were monitored every 8 hrs in M9 medium containing 15 g/L glycerol.

### 4.4.5 Applying dynamic control network to MA biosynthesis - down regulation in wild type strain

On the basis of the effectively dynamic up-regulation on the MA production, we next validated the dynamic down-regulation effect on the MA production by employing the MA-

induced asRNA interference on this system to redirect carbon flux to the shikimate pathway. Starting from the condensation of phosphoenolpyruvate (PEP) and erythrose 4-phosphate (E4P), shikimate pathway was restricted by the PEP availability (3%) due to the existence of various competing pathways, including the PTS sugar transport system (50%), glycolysis (15%), peptidoglycan synthesis (16%) and anapleurotic pathway (16%)[94]. During glycolysis, PEP flows into TCA cycle mainly by two pathways, PykA and PykF catalyzed conversion to pyruvate and then decarboxylated to acetyl-CoA, and Ppc catalyzed carboxylation to OAA (Figure 2a). To render MA biosensor mediated accumulation of intracellular PEP, we first designed asRNAs targeting *pykA* and *pykF*, put them under the control of $P_{MA}$ promoter respectively and introduced them into the plasmid pZE-p$P_{LlacO-1}$-EP, generating plasmid pZE-p$P_{LlacO-1}$-EP-p$P_{MA}$-*aspykA*(100)-p$P_{MA}$-*aspykF*(100). When it was transferred into E. coli BW25113/F' with plasmid pSA-p$P_{LlacO-1}$-NC-p$P_{lpp}$-CatR, the resultant strain produced 131mg/L of MA at 48h without IPTG induction, which was 2.65-fold increase compared with that (49 mg/L) of the control strain without the MA induced dynamic control function. It also exhibited a similar trend of cell growth comparing with the control strain (Figure 4.8). These results showed that MA-induced up-regulation can be efficiently transduced into down-regulation by the coupled RNAi at the metabolic level, leading to better MA biosynthesis. The similar growth profile demonstrated that introduction of the genetic parts necessary for the down-regulation function did not cause any significant stress to cell growth. Next, we identified if the dynamic down-regulation would perform better than the static knockout group. Thus, we disrupted gene *pykA* and *pykF* from strain BW25113/F', generating permanent static knockout strain YYP2. Surprisingly, YYP2 carrying pZE-p$P_{LlacO-1}$-EP and pSA-p$P_{LlacO-1}$-NC-p$P_{lpp}$-CatR produced 288 mg/L MA at 48 hrs without IPTG induction, which was almost 2.2-fold higher than the titer (130.7 mg/L) of the

strain with dynamic down-regulation. produced by the double knockout strain YYP4 carrying pZE-p$P_{LlacO-1}$-EP and pSA-p$P_{LlacO-1}$-NC-p$P_{lpp}$-CatR (Figure 4.8). These results directly pointed that the dynamic down-regulation even performed worse than the corresponding static knockout strain. To further identify the reason, we further checked the growth profile of the YY2 based MA-producing strain and found that static knockout strain exhibited even higher end-point cell density and longer growth phase. These results implied that dynamic control of cellular metabolism was not necessarily better than the corresponding static control if the static control did not bring any negative impact on the cellular metabolism or cell growth.

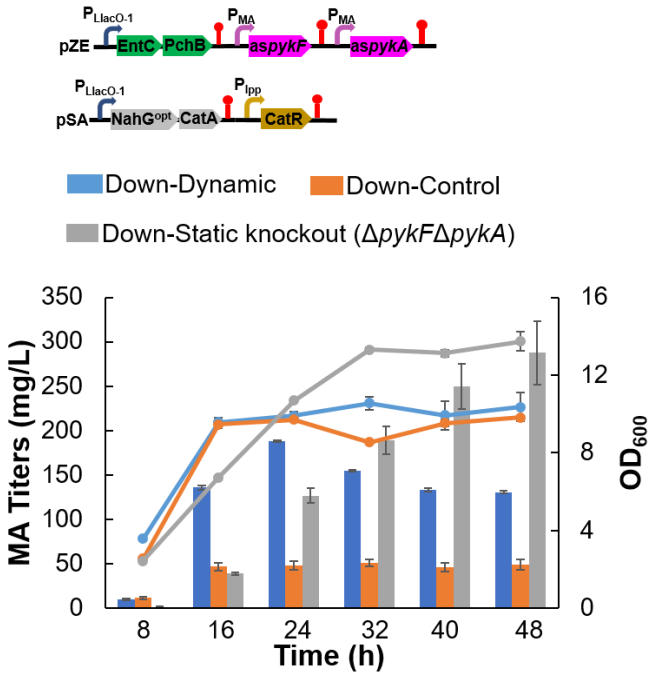


**Figure 4.8** MA production behavior by dynamic MA biosensor mediated down-regulation in wild type strain *E. coli* BW25113/F'. The productivity (cell density and MA titers) of *E. coli* strain BW25113/F' containing $P_{LlacO-1}$ promoter mediated EP module (p$P_{LlacO-1}$-EP, in *E. coli* BW25113/F') and $P_{MA}$ promoter mediated as*pykF* and as*pykA* (p$P_{LlacO-1}$-EP, $P_{MA}$-as*pykF*-$P_{MA}$-as*pykA* in *E. coli* BW25113/F'), as well as control strain YYP2 with *pykFpykA* knockout

($pP_{LlacO-1}$-EP, in *E. coli ⊿pykA ⊿pykF* BW25113/F') were monitored every 8 hrs in M9 medium containing 15 g/L glycerol.

### 4.4.6 Applying dynamic control network to MA biosynthesis - effect of knockouts on cell growth

To verify the importance of each gene for the cell growth, we knocked out all three genes individually and combinatorically. When the gene *pykA* was deleted, no significant growth retardation was observed when compared with the wild type strain (Figure 4.9). However, when the gene *pykF* was deleted, the cell density was even higher than the wild type strain and gene *pykA* knockout strains in late lag phase. When knocking out both *pykA* and *pykF*, the resultant strain showed a longer lag phase with higher end-point cell density than the wild type strain, which was consistent with the above growth profile during MA biosynthesis. However, when disrupting *ppc* alone, the cell density was greatly decreased by 2-fold than the wild type strain. Further disrupting *pykA* and *pykF* in the *ppc* knockout strain slightly restored the cell growth, but also showed significant growth retardation compared with the wild type strain (Figure 4.9). These results indicated that gene *ppc* is responsible for the major PEP consumption. Its disruption would introduce undesired burden to cellular metabolism by limiting the carbon source for cell growth.

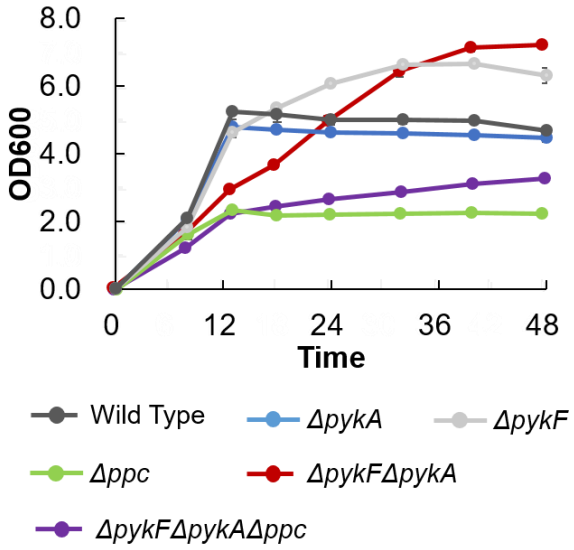


**Figure 4.9** Identification of cell growth-dependent genes by knocking out genes *pykF*, *pykF* and *ppc* individually and combinatorically. All the above data represented the average of three biological replicates, and error bars represented s.d.

### 4.4.7 Applying dynamic control network to MA biosynthesis - down regulation of *ppc* in *ΔpykA ΔpykF* strain

Based on the above results, we hypothesized that dynamic down-regulation of *ppc* instead of static control by permanent disruption would render the biological robustness to host by alleviating the metabolism stress and then support better MA biosynthesis. To verify this hypothesis, strain YYP2 (BW25113/F' containing *ΔpykA* and *ΔpykF*) would serve as the host strain for MA biosynthesis and gene *ppc* was left as the dynamic down-regulation target. When pZE-pP$_{LlacO-1}$-EP-pP$_{MA}$-*asppc* (100) and pSA-pP$_{LlacO-1}$-NC-pP$_{lpp}$-CatR were co-transferred into strain YYP2, the resulting strain produced 1282 mg/L MA at 48h without IPTG induction. As the control, we conducted the MA biosynthesis in strain YYP2 with pP$_{LlacO-1}$-*asppc* (100), which

provided a low-level static inhibition of *ppc* through leaking expression. Particularly, we also introduced the MA biosynthesis in strain YYP2 with *Δppc* (YYP3) and without carrying $pP_{MA}$-*asppc* (100), which provided a high-level static down-regulation. As the result in Figure 4.10, these two strains produced 484 mg/L and 114 mg/L MA, which were 2.7-fold and 11.2-fold less than the dynamic down-regulation strain containing $pP_{MA}$-*asppc* (100) (Fig 4.10a). To further

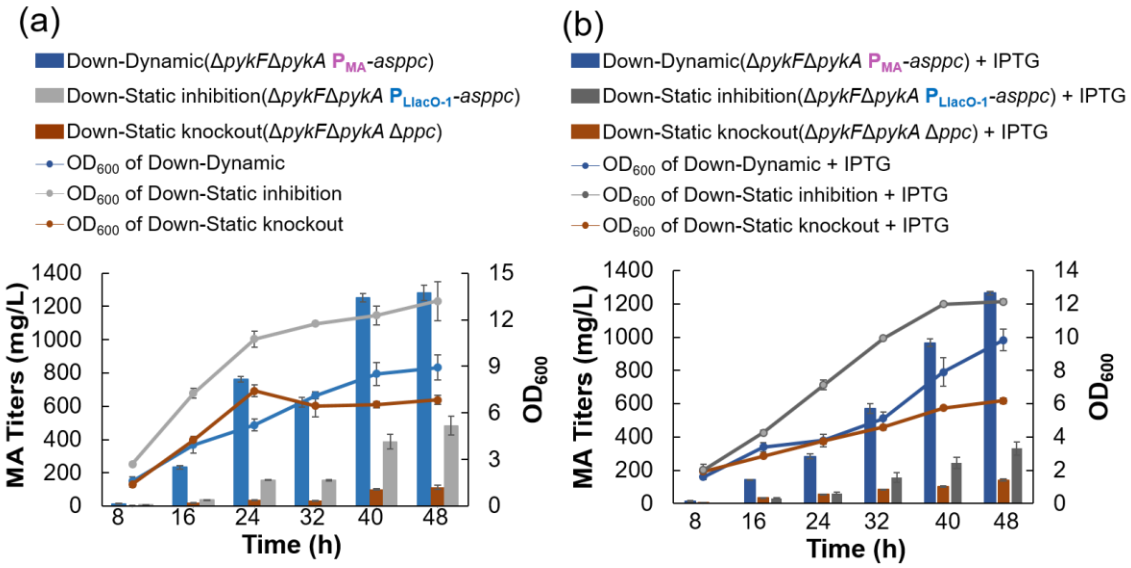


**Figure 4.10** MA production behavior by dynamic MA biosensor mediated down-regulation. (a) The productivity (cell density and MA titers) of dynamic down-regulation strain ($pP_{LlacO-1}$-EP, $pP_{MA}$-as*ppc*, in *E. coli Δ pykF Δ pykA* BW25113/F'), the static knockout strain ($pP_{LlacO-1}$-EP, in *E. coli Δ pykF Δ pykA Δ ppc* BW25113/F'), and the static inhibition strain containing $P_{LlacO-1}$ promoter mediated as*ppc* ($pP_{LlacO-1}$-EP, $pP_{LlacO-1}$-as*ppc*, in *E. coli Δ pykF Δ pykA* BW25113/F') were monitored every 8 hrs in M9 medium containing 15 g/L glycerol. (b) was sequentially corresponded with (a) by inducing 0.5mM IPTG. All the above data represented the average of three biological replicates, and error bars represented s.d.

compare the robustness of these strains, we also investigated the MA biosynthesis with the presence of sufficient IPTG (0.5 mM) which enabled fully expressed MA biosynthesis pathway (EP and NC module) in all strains and fully expressed *asppc* in the control strain containing $pP_{LlacO-1}$-*asppc* (100) as a moderate static inhibition. As the results (Figure 4.10b), the control strain with moderate-level static inhibition produced 331 mg/L MA and the one with *Δppc* produced even less (141 mg/L), while the strain with dynamic control still performed 1264 mg/L MA, which showed 3.82-fold and 8.96-fold increases compared to the control strains. Furthermore, in addition, in the both conditions (with or without IPTG), we observed that the dynamic down-regulation system was able to improve the cell growth compared with the control strain containing *Δppc* and provided longer growth phase compared both control strains.

### 4.4.8 Applying dynamic control network to MA biosynthesis - up regulation in *ΔpykA ΔpykF* strain

To validate the effect of the MA biosensor mediated up-regulation in the same background strain YYP2, the plasmids pZE-$pP_{MA}$-EP and pSA-$pP_{LlacO-1}$-NC-$pP_{lpp}$-CatR were co-transformed into *E. coli* YYP2, the resultant strain obtained 1157 mg/L at 48 h without IPTG induction, which was 3.7-fold increase compared with the control strain YYP2 (316 mg/L) containing the plasmids pZE-$pP_{LlacO-1}$-EP and pSA-$pP_{LlacO-1}$-NC-$pP_{lpp}$-CatR (Figure 4.11a). Similarly, when both the strains were induced with 0.5 mM IPTG, the resultant strain obtained 2.65-fold increase (1044 mg/L V.S. 395 mg/L) of MA production comparing to the $P_{LlacO-1}$-EP mediated control strain (Figure 4.11b). Notably, the dynamic up-regulation extended the growth phase at both conditions with or without IPTG, although less cell density was reached. These results

reconfirmed that the increased MA production was due to the dynamic up-regulation of EP module.

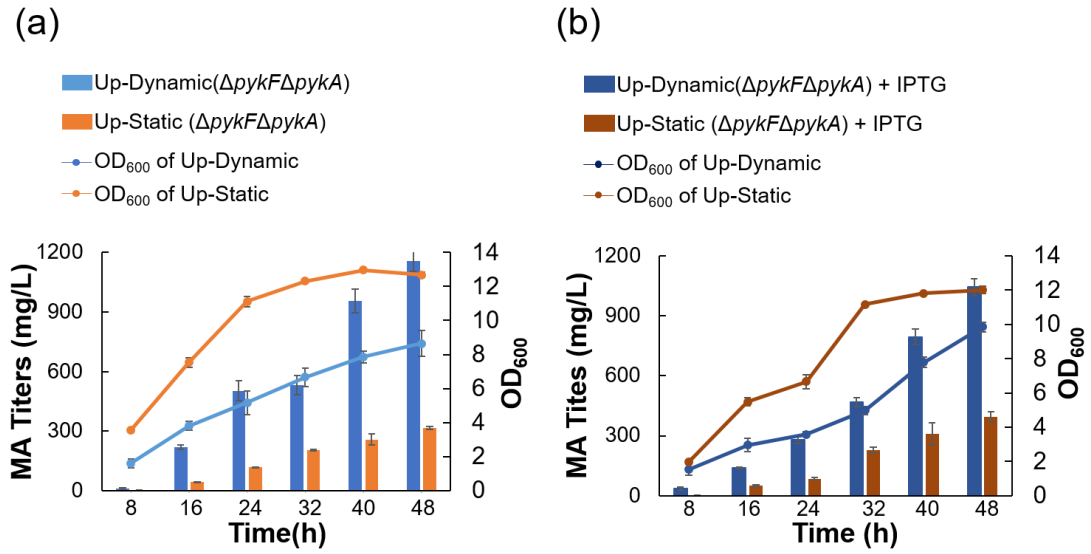


**Figure 4.11** MA production behavior by dynamic MA biosensor mediated up-regulation. (a) The productivity (cell density and MA titers) of dynamic up-regulation strain ($pP_{MA}$-EP, in *E. coli ΔpykF ΔpykA*BW25113/F'), the static strain ($pP_{LlacO-1}$-EP, in *E. coli ΔpykF ΔpykA*BW25113/F') were monitored every 8 hrs in M9 medium containing 15 g/L glycerol. (b) was sequentially corresponded with (a) by inducing 0.5mM IPTG. All the above data represented the average of three biological replicates, and error bars represented s.d.

### 4.4.9 Applying dynamic control network to MA biosynthesis – bi-functional regulation in *ΔpykA ΔpykF* strain

Given the success in the MA responsive promoter driven up-regulation of metabolic pathway on plasmid and down-regulation of competing pathway on genome, in the next step, we combined up- and down-regulation to develop the artificial dynamic regulatory network in *E.*

*coli*. We co-transformed plasmids pZE-pP$_{MA}$-EP-pP$_{MA}$-as*ppc*(100) and pSA-pP$_{LlacO-1}$-NC-pP$_{lpp}$-CatR into *E. coli* YYP2, the resultant strain produced 1862 mg/L MA at 48h without IPTG induction, exhibiting 3.85-fold increase of MA production (384 mg/L) than the control strain YYP2 carrying pZE-pP$_{LlacO-1}$-EP-pP$_{LlacO-1}$-asppc(100) and pSA-pP$_{LlacO-1}$-NC-pP$_{lpp}$-CatR and 16.31-fold increase of MA production (114.1 mg/L) than the control strain YYP3 carrying pZE-pP$_{LlacO-1}$-EP and pSA-pP$_{LlacO-1}$-NC-pP$_{lpp}$-CatR (Figure 4.12a). Similarly, when inducing with 0.5 mM IPTG, as shown in Figure 4.12b, the strain with simultaneous up-and down-regulation exhibited a 4.47-fold increase (1478 mg/L V.S. 331 mg/L) of MA production at 48h comparing to the pP$_{LlacO-1}$-as*ppc* mediated control strain in *E.coli* YYP2, and a 10.48-fold increase (1478 mg/L V.S. 141 mg/L) of MA production at 48h comparing to the control strain in *E.coli* YY3. These results determined that the artificial dynamic regulatory network possesses great potential to mimic the natural regulatory system by autonomously up-regulating the desirable pathway genes and down-regulating the native competing pathway genes responsive to the changing cellular physiological state for optimal microbial production.

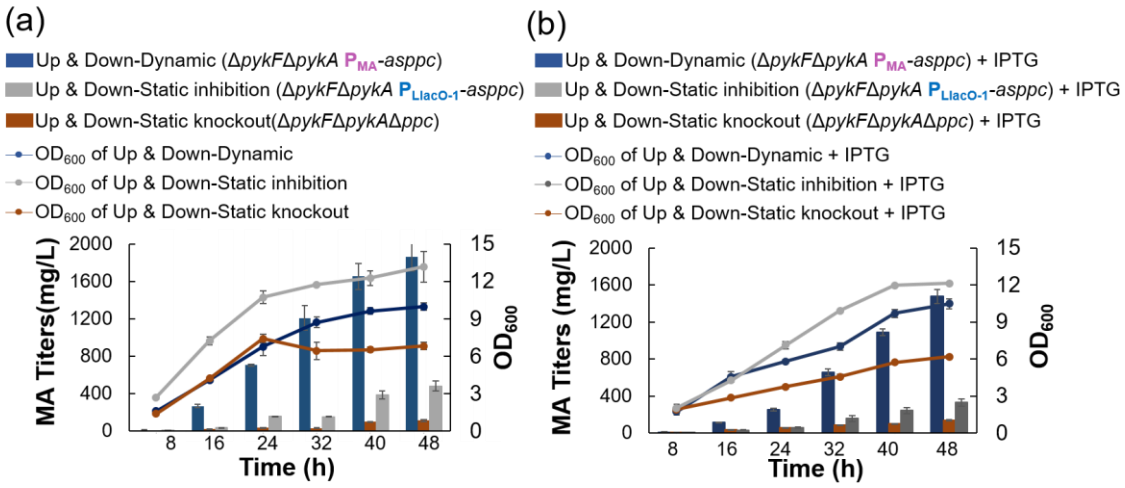


**Figure 4.12** MA production behavior of simultaneous up- and down-regulation mediated by dynamic MA biosensor. (a) The P$_{MA}$ promoter mediated EP module and P$_{LlacO-1}$ promoter

mediated as*ppc* (p$P_{LlacO-1}$-EP, $P_{MA}$-as*ppc*) were combined and expressed into the strain YYP2 (*E. coli ΔpykA ΔpykF*BW25113/F'). The productivity (cell density and MA titers) of this generated strain was compared with the static knockout strain (p$P_{LlacO-1}$-EP, in *E. coli ΔpykF ΔpykA Δppc* BW25113/F') and the static inhibition strain containing $P_{LlacO-1}$ promoter mediated as*ppc* (p$P_{LlacO-1}$-EP, p$P_{LlacO-1}$-as*ppc* in *E. coli ΔpykF ΔpykA* BW25113/F') every 8 hrs in M9 medium containing 15 g/L glycerol. (b) was sequentially corresponded with the (a) with 0.5mM IPTG induction. All the above data represented the average of three biological replicates, and error bars represented s.d.

**4.5 Discussion**

In summary, to blend in cellular complexity and achieve metabolic balance, we constructed a dynamic regulation system in *E. coli* by exploiting a noncognate muconic acid biosensor CatR that allowed MA dose-dependent up-regulation of plasmid-borne metabolic pathways and downregulation of chromosomal competing pathways. When implemented in *E. coli* cells, we observed mildly compromised cell growth but significantly enhanced bioproduction of muconic acid (1.8 g/L), which is substantially higher than static control by IPTG-induced system in either wild type or knockout strains. Given multiple competing pathways involved, knocking out of non-essential genes (*pykA* and *pykF*) and dynamic knocking down of essential genes (*ppc*) that are coupled to cell growth simultaneously restored cell growth and redistributed carbon fluxes to MA in a growth-dependent manner. Sustainable accumulation of end-products would potentially afford optimal production by redirecting carbon sources to MA that could otherwise be used for biomass. Particularly, introduction of end-product biosensors mediated up-regulation and asRNA interference could serve as a general paradigm of dynamic push and pull, and holds great

promise for broad utilities of dynamic control systems in metabolic engineering. Other newly well-documented repression methods like programable CRISPRi and protein degradation could be anchored in dynamic control systems. This study also underscores some important issues for applicability of dynamic control systems, like efficient biosynthetic routes and no intermediate accumulation or rate-limiting steps. As we demonstrated here, optimization of EP and NC module permitted carbon fluxes channeling into muconic acid, even without enhancing shikimate pathway genes. Applications of dynamic control systems would potentially develop high-performance microbial strains with autonomous production behaviors[95].

# CHAPTER 5

## SUPPORTING INFORMATION OF CHAPTER 4

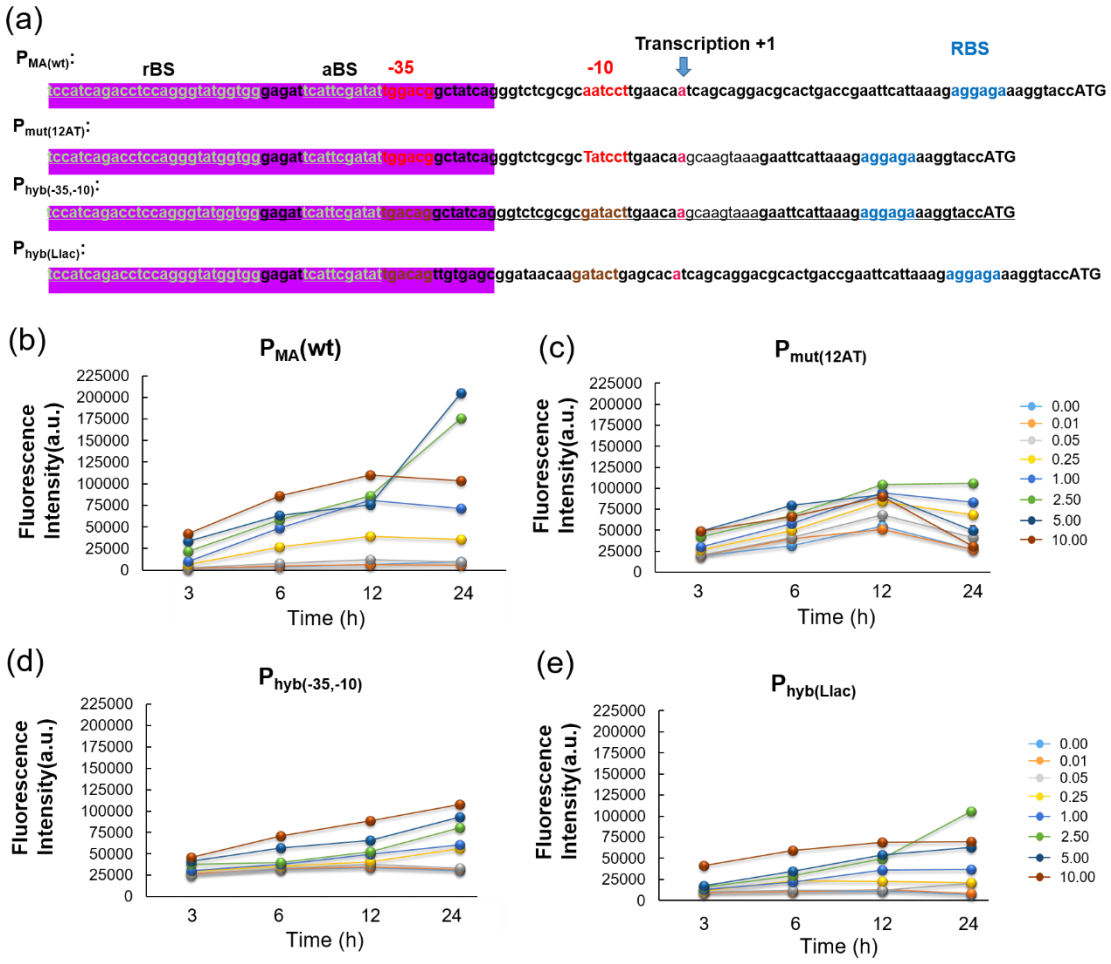


**Figure 5.1** Development of hybrid promoters responsive to muconic acid (MA). (a) Design of the hybrid $P_{MA}$ promoters. The DNA sequence in the purple boxes contained the CatR repression binding site (rBS) and activation binding site (aBS). The sequences in red indicated the −35 and −10 regions of the wild type $P_{MA}$ promoter. Transcript start sites were colored pink and pointed by blue arrow. $P_{mut(12AT)}$ represented a mutated T from A at the -12 position of wild type $P_{MA}$ promoter. $P_{hyb(-35,-10)}$ represented the replaced -35 and -10 regions of the wild type $P_{MA}$ promoter

with those of $P_{LlacO-1}$. $P_{hyb(Llac)}$ represented the completely replaced promoter sequence of the wild type $P_{MA}$ promoter by $P_{LlacO-1}$ promoter sequence spanning from -35 to -10 region. Ribosome binding sites were colored in Blue. (b-e) Dosage response of the developed MA biosensors to exogenous MA. Biosensor plasmids pZE-p$P_{MA(wt)}$-eGFP-p$P_{lpp}$-CatR (b), pZE-p$P_{mut(12AT)}$-eGFP-p$P_{lpp}$-CatR (c), pZE-p$P_{hyb(-35,-10)}$-eGFP-p$P_{lpp}$-CatR (d) and pZE-p$P_{hyb(Llac)}$-eGFP-p$P_{lpp}$-CatR (e) were transformed into *E. coli* BW25113/F', respectively. Various amounts of MA were added into the medium before the inoculation, and eGFP fluorescence was measured after incubation at 37 °C and 290 rpm for 24 hrs.

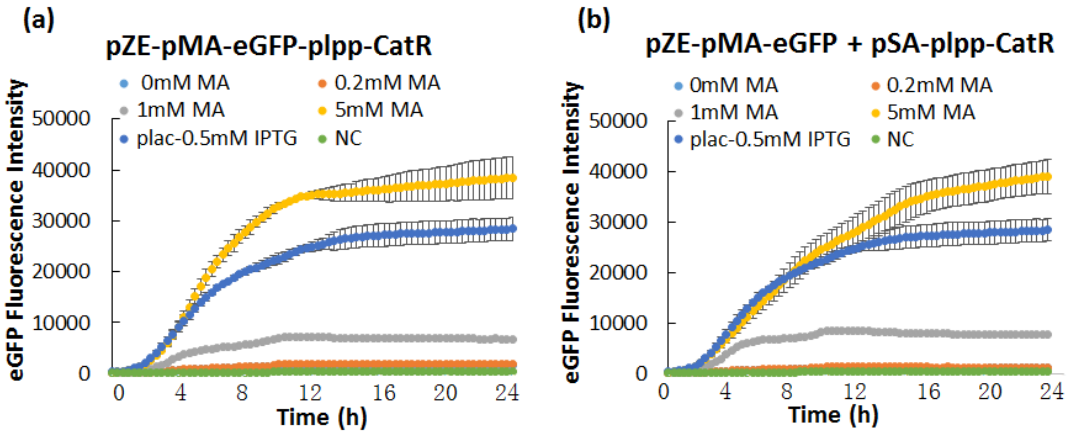


**Figure 5.2** The effect of CatR abundance on the $P_{MA}$ dynamic range. (a) The $P_{lpp}$-CatR and $P_{MA}$-eGFP cassettes were expressed in the same high copy number plasmid pZE12-luc. (b) The $P_{lpp}$-CatR cassette was expressed separately in a low copy number plasmid pSA74. 2 % of overnight culture of *E. coli* BW25113/F' harboring various plasmids was inoculated into 200 uL LB medium. MA was titrated with different concentration (0, 0.2, 1.0, 5.0 mM). Plac represented the *E. coli* BW25113/F' harboring pZE-p$P_{LlacO-1}$-eGFP induced with 0.5mM IPTG and the eGFP intensity was served as positive control. The NC represented the *E. coli* BW25113/F' harboring empty pZE-luc12 and the eGFP intensity was served as negative control. Fluorescence was

measured at each 20 min at 37 °C for 24 hrs. Data were obtained from the average of three biological replicates, and error bars represented standard deviations.

# CHAPTER 6

## CONCLUSION

In conclusion, we have shown how to engineer the static and dynamic control of the microbial biosynthesis pathways to improve the desired production. Some of the results showed that dynamic control strategy has potential to be applied into other biosynthesis pathways to increase the production of desired compounds. Among these studies, we will discuss the relative applicability as following:

Firstly, to break the metabolic homeostasis in the host cells, people have developed a series of static control approaches in the genome level to constrain the endogenous metabolism and overproduce the heterologous biosynthesis pathways such as Multiplex Automated Genome Engineering (MAGE), its derivatives Microarray oligonucleotide-MAGE (MO-MAGE)[96], Coselection MAGE (CoS-MAGE)[97], Conjugative Assembly Genome Engineering (CAGE)[98, 99], and clustered regularly interspaced palindromic repeats (CRISPR)/Cas9-mediated gene deletion and integration[100]. Even though these strategies have proven effective and reduced the required labor and time for engineering microbes with multiple genome manipulations, the lethal effect of knockout strategy on the essential genes which are critical for cell viability and active growth, greatly limits the cell growth and protein expression. Thus, it is important to develop the heterologous genetic regulators and apply them into the static pathway control. The previous studies have reported some successful applications, such as hfq-mediated RNAi[44] and dCas9-mediated gene inhibition[101]. However, these methods inevitably introduced a foreign protein to assist the asRNAs to recognize the target genes, resulting in a complex genetic manipulation.

Thus, in our studies, we reported a simple asRNA design to achieve controllable inhibition efficiency by changing the asRNA binding length, the asRNA recognition sites and asRNA abundance. Compared with the previous studies, our approach was easier to operate because of its smaller size, fewer elements and comparable inhibition efficiency. These advantages were also important in the design of the dynamic control network.

Secondly, even though the developed static control strategies have achieved critical success on alleviating the metabolic imbalance and improveing heterologous production, these static controls on enzyme levels still exhibited disadvantages on the inability to sense perturbations and adjust unfavorable metabolic states toward the designed goal[92]. Comparing with the static control, native metabolic pathways generally use dynamic regulatory networks to compensate the changed conditions by altering fluxes[14]. Thus, engineering dynamic control system represents a new frontier of metabolic engineering and synthetic biology. However, as we discussed in the previous chapters, the previously demonstrated applications were mainly mono-functional regulation system with only up-regulation or only down-regulation. Their regulation mainly took place on the transcriptional level. Compared with the previous design, we applied a sensor-regulator to control both the desired pathway genes and designed asRNAs. When the metabolites accumulated, it would be sensed by the system and triggered the desired pathway genes to achieve up-regulation function. When this up-regulation was used to synthesize asRNAs, the activated asRNAs would inhibit the multiple competing pathway genes to achieve down-regulation function (Figure 2). Thus, our dynamic control network was a multi-functional regulation system. And it also performed a simultaneous up-regulation and down-regulation in an orthogonal manner. Furthermore, in our engineered system provided a prototype of dynamic

control network, other down-regulation approaches such as dCas9 strategy, can be introduced into this system to program diversity of dynamic effects.

Finally, based on the result in the chapter 4, the effect of dynamic control system on improving the microbial production was not necessary better than the static knockout strain. The dynamic control system only exhibited effective when the corresponding static control approach have negative impacts on the central cellular metabolism. Particularly, this work also improved our understanding of the role of the PEP metabolic node in the cellular metabolism. The previous report demonstrated that the *ppc* knockout strain didn't show improved production when PEP as the precursor of desired pathway. Here, we demonstrated that the dynamic control on the PEP metabolic node could achieve autonomously intelligent distribution of carbon flux from the biomass synthesis to the microbial production by sensing the intracellular metabolites. This finding can also be extended to enhance the biosynthesis of shikimate pathway derived products and other PEP-dependent compounds.

## REFERENCES


1. Solomon, K.V., Moon, T.S., Ma, B., Sanders, T.M. & Prather, K.L. Tuning primary metabolism for heterologous pathway productivity. *ACS synthetic biology* **2**, 126-135 (2013).
2. Feist, A.M., Herrgard, M.J., Thiele, I., Reed, J.L. & Palsson, B.O. Reconstruction of biochemical networks in microorganisms. *Nature reviews. Microbiology* **7**, 129-143 (2009).
3. Lutke-Eversloh, T. & Stephanopoulos, G. Combinatorial pathway analysis for improved L-tyrosine production in Escherichia coli: identification of enzymatic bottlenecks by systematic gene overexpression. *Metabolic engineering* **10**, 69-77 (2008).
4. Blankschien, M.D., Clomburg, J.M. & Gonzalez, R. Metabolic engineering of Escherichia coli for the production of succinate from glycerol. *Metabolic engineering* **12**, 409-419 (2010).
5. Lin, Y., Sun, X., Yuan, Q. & Yan, Y. Extending shikimate pathway for the production of muconic acid and its precursor salicylic acid in Escherichia coli. *Metabolic engineering* **23**, 62-69 (2014).
6. Lin, Y., Shen, X., Yuan, Q. & Yan, Y. Microbial biosynthesis of the anticoagulant precursor 4-hydroxycoumarin. *Nat Commun* **4**, 2603 (2013).
7. Salis, H.M., Mirsky, E.A. & Voigt, C.A. Automated design of synthetic ribosome binding sites to control protein expression. *Nature biotechnology* **27**, 946-950 (2009).
8. Hammer, K., Mijakovic, I. & Jensen, P.R. Synthetic promoter libraries--tuning of gene expression. *Trends in biotechnology* **24**, 53-55 (2006).
9. Schuetz, R., Zamboni, N., Zampieri, M., Heinemann, M. & Sauer, U. Multidimensional optimality of microbial metabolism. *Science* **336**, 601-604 (2012).
10. Wegner, A., Meiser, J., Weindl, D. & Hiller, K. How metabolites modulate metabolic flux. *Current opinion in biotechnology* **34**, 16-22 (2015).
11. Fung, E. et al. A synthetic gene-metabolic oscillator. *Nature* **435**, 118-122 (2005).
12. Zhang, F., Carothers, J.M. & Keasling, J.D. Design of a dynamic sensor-regulator system for production of chemicals and fuels derived from fatty acids. *Nat Biotechnol* **30**, 354-359 (2012).
13. Xu, P., Li, L.Y., Zhang, F.M., Stephanopoulos, G. & Koffas, M. Improving fatty acids production by engineering dynamic pathway regulation and metabolic control. *P Natl Acad Sci USA* **111**, 11299-11304 (2014).
14. Holtz, W.J. & Keasling, J.D. Engineering static and dynamic control of synthetic pathways. *Cell* **140**, 19-23 (2010).
15. Zhang, A. & Yang, S.T. Engineering Propionibacterium acidipropionici for enhanced propionic acid tolerance and fermentation. *Biotechnol Bioeng* **104**, 766-773 (2009).
16. Yang, Y., Lin, Y., Li, L., Linhardt, R.J. & Yan, Y. Regulating malonyl-CoA metabolism via synthetic antisense RNAs for enhanced biosynthesis of natural products. *Metab Eng* **29**, 217-226 (2015).

17. Han, A.R. et al. Development of a Streptomyces venezuelae-based combinatorial biosynthetic system for the production of glycosylated derivatives of doxorubicin and its biosynthetic intermediates. *Applied and environmental microbiology* **77**, 4912-4923 (2011).
18. Olano, C., Mendez, C. & Salas, J.A. Molecular insights on the biosynthesis of antitumour compounds by actinomycetes. *Microb Biotechnol* **4**, 144-164 (2011).
19. Griffin, M.O., Fricovsky, E., Ceballos, G. & Villarreal, F. Tetracyclines: a pleitropic family of compounds with promising therapeutic properties. Review of the literature. *Am J Physiol Cell Physiol* **299**, C539-548 (2010).
20. Yan, Y., Li, Z. & Koffas, M.A. High-yield anthocyanin biosynthesis in engineered Escherichia coli. *Biotechnology and bioengineering* **100**, 126-140 (2008).
21. Leonard, E. et al. Strain improvement of recombinant Escherichia coli for efficient production of plant flavonoids. *Mol Pharm* **5**, 257-265 (2008).
22. Dahl, R.H. et al. Engineering dynamic pathway regulation using stress-response promoters. *Nature Biotechnology* **31**, 1039-+ (2013).
23. Xu, P. et al. Modular optimization of multi-gene pathways for fatty acids production in E. coli. *Nat Commun* **4**, 1409 (2013).
24. Zha, W., Rubin-Pitel, S.B., Shao, Z. & Zhao, H. Improving cellular malonyl-CoA level in Escherichia coli via metabolic engineering. *Metabolic engineering* **11**, 192-198 (2009).
25. Koirala, N., Pandey, R.P., Van Thang, D., Jung, H.J. & Sohng, J.K. Glycosylation and subsequent malonylation of isoflavonoids in E. coli: strain development, production and insights into future metabolic perspectives. *J Ind Microbiol Biotechnol* (2014).
26. Malla, S., Koffas, M.A., Kazlauskas, R.J. & Kim, B.G. Production of 7-O-methyl aromadendrin, a medicinally valuable flavonoid, in Escherichia coli. *Applied and environmental microbiology* **78**, 684-694 (2012).
27. Rathnasingh, C. et al. Production of 3-hydroxypropionic acid via malonyl-CoA pathway using recombinant Escherichia coli strains. *J Biotechnol* **157**, 633-640 (2012).
28. Janssen, H.J. & Steinbuchel, A. Fatty acid synthesis in Escherichia coli and its applications towards the production of fatty acid based biofuels. *Biotechnol Biofuels* **7**, 7 (2014).
29. Lussier, F.X., Colatriano, D., Wiltshire, Z., Page, J.E. & Martin, V.J. Engineering microbes for plant polyketide biosynthesis. *Comput Struct Biotechnol J* **3**, e201210020 (2012).
30. Causey, T.B., Shanmugam, K.T., Yomano, L.P. & Ingram, L.O. Engineering Escherichia coli for efficient conversion of glucose to pyruvate. *Proceedings of the National Academy of Sciences of the United States of America* **101**, 2235-2240 (2004).
31. Cronan, J.E. & Thomas, J. Bacterial fatty acid synthesis and its relationships with polyketide synthetic pathways. *Methods Enzymol* **459**, 395-433 (2009).
32. Davis, M.S., Solbiati, J. & Cronan, J.E., Jr. Overproduction of acetyl-CoA carboxylase activity increases the rate of fatty acid biosynthesis in Escherichia coli. *The Journal of biological chemistry* **275**, 28593-28598 (2000).
33. Santos, C.N., Koffas, M. & Stephanopoulos, G. Optimization of a heterologous pathway for the production of flavonoids from glucose. *Metabolic engineering* **13**, 392-400 (2011).

34. Nakashima, N., Tamura, T. & Good, L. Paired termini stabilize antisense RNAs and enhance conditional gene silencing in Escherichia coli. *Nucleic acids research* **34**, e138 (2006).
35. Henz, S.R. et al. Distinct expression patterns of natural antisense transcripts in Arabidopsis. *Plant Physiol* **144**, 1247-1255 (2007).
36. Scalcinati, G. et al. Dynamic control of gene expression in Saccharomyces cerevisiae engineered for the production of plant sesquitepene alpha-santalene in a fed-batch mode. *Metabolic engineering* **14**, 91-103 (2012).
37. Storz, G., Vogel, J. & Wassarman, K.M. Regulation by small RNAs in bacteria: expanding frontiers. *Mol Cell* **43**, 880-891 (2011).
38. Thomason, M.K. & Storz, G. Bacterial Antisense RNAs: How Many Are There, and What Are They Doing? *Annual Review of Genetics, Vol 44* **44**, 167-188 (2010).
39. Wang, B. & Kuramitsu, H.K. Inducible antisense RNA expression in the characterization of gene functions in Streptococcus mutans. *Infect Immun* **73**, 3568-3576 (2005).
40. Ji, Y. et al. Validation of antibacterial mechanism of action using regulated antisense RNA expression in Staphylococcus aureus. *FEMS Microbiol Lett* **231**, 177-184 (2004).
41. Sharma, V., Sakai, Y., Smythe, K.A. & Yokobayashi, Y. Knockdown of recA gene expression by artificial small RNAs in Escherichia coli. *Biochem Biophys Res Commun* **430**, 256-259 (2013).
42. Tummala, S.B., Welker, N.E. & Papoutsakis, E.T. Design of antisense RNA constructs for downregulation of the acetone formation pathway of Clostridium acetobutylicum. *J Bacteriol* **185**, 1923-1934 (2003).
43. Mellin, J.R. et al. A riboswitch-regulated antisense RNA in Listeria monocytogenes. *Proceedings of the National Academy of Sciences of the United States of America* **110**, 13132-13137 (2013).
44. Na, D. et al. Metabolic engineering of Escherichia coli using synthetic small regulatory RNAs. *Nat Biotechnol* **31**, 170-174 (2013).
45. Yoo, S.M., Na, D. & Lee, S.Y. Design and use of synthetic regulatory small RNAs to control gene expression in Escherichia coli. *Nature Protocols* **8**, 1694-1707 (2013).
46. Solomon, K.V., Sanders, T.M. & Prather, K.L. A dynamic metabolite valve for the control of central carbon metabolism. *Metabolic engineering* **14**, 661-671 (2012).
47. Kang, Z., Wang, X., Li, Y., Wang, Q. & Qi, Q. Small RNA RyhB as a potential tool used for metabolic engineering in Escherichia coli. *Biotechnol Lett* **34**, 527-531 (2012).
48. Lutz, R. & Bujard, H. Independent and tight regulation of transcriptional units in Escherichia coli via the LacR/O, the TetR/O and AraC/I1-I2 regulatory elements. *Nucleic Acids Res* **25**, 1203-1210 (1997).
49. Shen, C.R. & Liao, J.C. Metabolic engineering of Escherichia coli for 1-butanol and 1-propanol production via the keto-acid pathways. *Metabolic engineering* **10**, 312-320 (2008).
50. Huo, Y.X. et al. Conversion of proteins into biofuels by engineering nitrogen flux. *Nat Biotechnol* **29**, 346-U160 (2011).
51. Leonard, E., Chemler, J., Lim, K.H. & Koffas, M.A. Expression of a soluble flavone synthase allows the biosynthesis of phytoestrogen derivatives in Escherichia coli. *Applied microbiology and biotechnology* **70**, 85-91 (2006).

52. Lim, C.G., Fowler, Z.L., Hueller, T., Schaffer, S. & Koffas, M.A. High-yield resveratrol production in engineered Escherichia coli. *Applied and environmental microbiology* **77**, 3451-3460 (2011).
53. Leonard, E., Yan, Y.J. & Koffas, M.A.G. Functional expression of a P450 flavonoid hydroxylase for the biosynthesis of plant-specific hydroxylated flavonols in Escherichia coli. *Metabolic engineering* **8**, 172-181 (2006).
54. Yan, Y., Chemler, J., Huang, L., Martens, S. & Koffas, M.A. Metabolic engineering of anthocyanin biosynthesis in Escherichia coli. *Applied and environmental microbiology* **71**, 3617-3623 (2005).
55. Yan, Y.J., Kohli, A. & Koffas, M.A.G. Biosynthesis of natural flavanones in Saccharomyces cerevisiae. *Applied and environmental microbiology* **71**, 5610-5613 (2005).
56. Rapp, M. et al. Experimentally based topology models for E-coli inner membrane proteins. *Protein Sci* **13**, 937-945 (2004).
57. Livak, K.J. & Schmittgen, T.D. Analysis of relative gene expression data using real-time quantitative PCR and the 2(-Delta Delta C(T)) Method. *Methods* **25**, 402-408 (2001).
58. Xu, P. et al. Design and kinetic analysis of a hybrid promoter-regulator system for malonyl-CoA sensing in Escherichia coli. *ACS Chem Biol* **9**, 451-458 (2014).
59. Minkler, P.E., Kerner, J., Kasumov, T., Parland, W. & Hoppel, C.L. Quantification of malonyl-coenzyme A in tissue specimens by high-performance liquid chromatography/mass spectrometry. *Anal Biochem* **352**, 24-32 (2006).
60. Onorato, J.M. et al. Liquid-liquid extraction coupled with LC/MS/MS for monitoring of malonyl-CoA in rat brain tissue. *Anal Bioanal Chem* **397**, 3137-3142 (2010).
61. Patnaik, R., Roof, W.D., Young, R.F. & Liao, J.C. Stimulation of glucose catabolism in Escherichia coli by a potential futile cycle. *Journal of bacteriology* **174**, 7527-7532 (1992).
62. Crosby, H.A., Rank, K.C., Rayment, I. & Escalante-Semerena, J.C. Structure-guided expansion of the substrate range of methylmalonyl coenzyme A synthetase (MatB) of Rhodopseudomonas palustris. *Applied and environmental microbiology* **78**, 6619-6629 (2012).
63. Shi, S., Chen, Y., Siewers, V. & Nielsen, J. Improving production of malonyl coenzyme A-derived metabolites by abolishing Snf1-dependent regulation of Acc1. *MBio* **5**, e01130-01114 (2014).
64. Lee, S., Lee, S., Yoon, Y.J. & Lee, J. Enhancement of long-chain fatty acid production in Escherichia coli by coexpressing genes, including fabF, involved in the elongation cycle of fatty acid biosynthesis. *Appl Biochem Biotechnol* **169**, 462-476 (2013).
65. Price, A.C. et al. Inhibition of beta-ketoacyl-acyl carrier protein synthases by thiolactomycin and cerulenin. Structure and mechanism. *The Journal of biological chemistry* **276**, 6551-6559 (2001).
66. Nakashima, N. & Tamura, T. Conditional gene silencing of multiple genes with antisense RNAs and generation of a mutator strain of Escherichia coli. *Nucleic acids research* **37**, e103 (2009).
67. Wu, J.J., Yu, O., Du, G.C., Zhou, J.W. & Chen, J. Fine-Tuning of the Fatty Acid Pathway by Synthetic Antisense RNA for Enhanced (2S)-Naringenin Production from L-Tyrosine in Escherichia coli. *Applied and environmental microbiology* **80**, 7283-7292 (2014).

68. Weintraub, H., Izant, J.G. & Harland, R.M. Anti-Sense Rna as a Molecular Tool for Genetic-Analysis. *Trends Genet* **1**, 22-25 (1985).
69. Chen, G.Z., Patten, C.L. & Schellhorn, H.E. Controlled expression of an rpoS antisense RNA can inhibit RpoS function in Escherichia coli. *Antimicrob Agents Ch* **47**, 3485-3493 (2003).
70. Yin, D.Z. & Ji, Y.D. Genomic analysis using conditional phenotypes generated by antisense RNA. *Curr Opin Microbiol* **5**, 330-333 (2002).
71. Rasmussen, L.C.V., Sperling-Petersen, H.U. & Mortensen, K.K. Hitting bacteria at the heart of the central dogma: sequence-specific inhibition. *Microb Cell Fact* **6** (2007).
72. Carpousis, A.J. Degradation of targeted mRNAs in Escherichia coli: regulation by a small antisense RNA. *Gene Dev* **17**, 2351-2355 (2003).
73. Wagner, E.G.H., Altuvia, S. & Romby, P. Antisense RNAs in bacteria and their genetic elements. *Adv Genet* **46**, 361-398 (2002).
74. Tilley, L.D. et al. Gene-specific effects of antisense phosphorodiamidate morpholino oligomer-peptide conjugates on Escherichia coli and Salmonella enterica serovar typhimurium in pure culture and in tissue culture. *Antimicrob Agents Ch* **50**, 2789-2796 (2006).
75. Ross, J.A., Ellis, M.J., Hossain, S. & Haniford, D.B. Hfq restructures RNA-IN and RNA-OUT and facilitates antisense pairing in the Tn10/IS10 system. *Rna* **19**, 670-684 (2013).
76. Cruz, C. & Houseley, J. Endogenous RNA interference is driven by copy number. *Elife* **3** (2014).
77. Liu, D., Xiao, Y., Evans, B.S. & Zhang, F. Negative feedback regulation of fatty acid production based on a malonyl-CoA sensor-actuator. *ACS synthetic biology* **4**, 132-140 (2015).
78. Collier, J. Epigenetic regulation of the bacterial cell cycle. *Current opinion in microbiology* **12**, 722-729 (2009).
79. Berkhout, J., Bruggeman, F.J. & Teusink, B. Optimality principles in the regulation of metabolic networks. *Metabolites* **2**, 529-552 (2012).
80. Avalos, J.L., Fink, G.R. & Stephanopoulos, G. Compartmentalization of metabolic pathways in yeast mitochondria improves the production of branched-chain alcohols. *Nature biotechnology* **31**, 335-341 (2013).
81. Castellana, M. et al. Enzyme clustering accelerates processing of intermediates through metabolic channeling. *Nature biotechnology* **32**, 1011-1018 (2014).
82. Dueber, J.E. et al. Synthetic protein scaffolds provide modular control over metabolic flux. *Nature biotechnology* **27**, 753-759 (2009).
83. Zhang, K., Sawaya, M.R., Eisenberg, D.S. & Liao, J.C. Expanding metabolism for biosynthesis of nonnatural alcohols. *Proceedings of the National Academy of Sciences* **105**, 20653-20658 (2008).
84. Alper, H., Fischer, C., Nevoigt, E. & Stephanopoulos, G. Tuning genetic control through promoter engineering. *Proceedings of the National Academy of Sciences of the United States of America* **102**, 12678-12683 (2005).
85. Thomason, L.C., Costantino, N. & Court, D.L. E. coli genome manipulation by P1 transduction. *Current protocols in molecular biology* **Chapter 1**, Unit 1 17 (2007).
86. Doublet, B. et al. Antibiotic marker modifications of lambda Red and FLP helper plasmids, pKD46 and pCP20, for inactivation of chromosomal genes using PCR products in multidrug-resistant strains. *J Microbiol Meth* **75**, 359-361 (2008).

87. Lin, Y., Sun, X., Yuan, Q. & Yan, Y. Combinatorial biosynthesis of plant-specific coumarins in bacteria. *Metab Eng* **18**, 69-77 (2013).
88. Chugani, S.A., Parsek, M.R. & Chakrabarty, A.M. Transcriptional repression mediated by LysR-type regulator CatR bound at multiple binding sites. *J Bacteriol* **180**, 2367-2372 (1998).
89. Parsek, M.R., Kivisaar, M. & Chakrabarty, A.M. Differential DNA Bending Introduced by the Pseudomonas-Putida Lysr-Type Regulator, Catr, at the Plasmid-Borne Pheba and Chromosomal Catbc Promoters. *Molecular microbiology* **15**, 819-828 (1995).
90. Parsek, M.R., Ye, R.W., Pun, P. & Chakrabarty, A.M. Critical Nucleotides in the Interaction of a Lysr-Type Regulator with Its Target Promoter Region - Catbc Promoter Activation by Catr. *J Biol Chem* **269**, 11279-11284 (1994).
91. Chugani, S.A. et al. Activation of the catBCA promoter: Probing the interaction of CatR and RNA polymerase through in vitro transcription. *Journal of bacteriology* **179**, 2221-2227 (1997).
92. Hook-Barnard, I.G. & Hinton, D.M. The promoter spacer influences transcription initiation via sigma(70) region 1.1 of Escherichia coli RNA polymerase. *P Natl Acad Sci USA* **106**, 737-742 (2009).
93. Rugbjerg, P., Gence, H.J., Jensen, K., Sarup-Lytzen, K. & Sommer, M.O.A. Molecular Buffers Permit Sensitivity Tuning and Inversion of Riboswitch Signals. *ACS synthetic biology* **5**, 632-638 (2016).
94. Gosset, G. Improvement of Escherichia coli production strains by modification of the phosphoenolpyruvate: sugar phosphotransferase system. *Microbial Cell Factories* **4**, 1 (2005).
95. Lin, Y.H., Sun, X.X., Yuan, Q.P. & Yan, Y.J. Combinatorial biosynthesis of plant-specific coumarins in bacteria. *Metabolic engineering* **18**, 69-77 (2013).
96. Bonde, M.T. et al. Direct Mutagenesis of Thousands of Genomic Targets Using Microarray-Derived Oligonucleotides. *Acs Synth Biol* **4**, 17-22 (2015).
97. Wang, H.H. et al. Genome-scale promoter engineering by coselection MAGE. *Nat Methods* **9**, 591-+ (2012).
98. Ma, N.J., Moonan, D.W. & Isaacs, F.J. Precise manipulation of bacterial chromosomes by conjugative assembly genome engineering. *Nature Protocols* **9**, 2285-2300 (2014).
99. Isaacs, F.J. et al. Precise Manipulation of Chromosomes in Vivo Enables Genome-Wide Codon Replacement. *Science* **333**, 348-353 (2011).
100. Jinek, M. et al. A programmable dual-RNA-guided DNA endonuclease in adaptive bacterial immunity. *Science* **337**, 816-821 (2012).
101. Cress, B.F. et al. CRISPathBrick: Modular Combinatorial Assembly of Type II-A CRISPR Arrays for dCas9-Mediated Multiplex Transcriptional Repression in E-coli. *Acs Synth Biol* **4**, 987-1000 (2015).
102. Cress, B.F., Trantas, E.A., Ververidis, F., Linhardt, R.J. & Koffas, M.A. Sensitive cells: enabling tools for static and dynamic control of microbial metabolic pathways. *Current opinion in biotechnology* **36**, 205-214 (2015).